Article

SOURCE DATA | TRANSPARENT PROCESS | OPEN ACCESS

THE EMBO JOURNAL

TOC1 clock protein phosphorylation controls complex formation with NF-YB/C to repress hypocotyl growth

Jiapei Yan[1], Shibai Li[1,2], Yeon Jeong Kim[1], Qingning Zeng[1], Amandine Radziejwoski[3], Lei Wang[1,4], Yuko Nomura[5], Hirofumi Nakagami[5,6] & David E Somers[1,3,*]

Abstract

Plant photoperiodic growth is coordinated by interactions between circadian clock and light signaling networks. How post-translational modifications of clock proteins affect these interactions to mediate rhythmic growth remains unclear. Here, we identify five phosphorylation sites in the *Arabidopsis* core clock protein TIMING OF CAB EXPRESSION 1 (TOC1) which when mutated to alanine eliminate detectable phosphorylation. The TOC1 phosphomutant fails to fully rescue the clock, growth, and flowering phenotypes of the *toc1* mutant. Further, the TOC1 phosphomutant shows advanced phase, a faster degradation rate, reduced interactions with PHYTOCHROME-INTERACTING FACTOR 3 (PIF3) and HISTONE DEACETYLASE 15 (HDA15), and poor binding at predawn hypocotyl growth-related genes (PHGs), leading to a net derepression of hypocotyl growth. NUCLEAR FACTOR Y subunits B and C (NF-YB/C) stabilize TOC1 at target promoters, and this novel trimeric complex (NF-TOC1) acts as a transcriptional co-repressor with HDA15 to inhibit PIF-mediated hypocotyl elongation. Collectively, we identify a molecular mechanism suggesting how phosphorylation of TOC1 alters its phase, stability, and physical interactions with co-regulators to precisely phase PHG expression to control photoperiodic hypocotyl growth.

Keywords circadian; NUCLEAR FACTOR Y; phosphorylation; photomorphogenesis; TOC1

Subject Categories Chromatin, Transcription & Genomics; Plant Biology; Post-translational Modifications & Proteolysis

DOI 10.15252/embj.2021108684 | Received 9 May 2021 | Revised 5 October 2021 | Accepted 6 October 2021 | Published online 2 November 2021

The EMBO Journal (2021) 40: e108684

Introduction

The rotation of the earth on its axis subjects plants to diurnal photocycles which drive a cyclic pattern of many biological processes with a period of approximately 24 h. These rhythms are regulated by an internal circadian clock that enables plants to anticipate periodic environmental changes which allow optimal phasing of molecular, physiological, and behavioral responses to specific times of day (Dunlap, 1999; Harmer *et al*, 2001; Yakir *et al*, 2007). Light is the most important environmental cue in the entrainment of the clock, facilitating a stable phase relationship with external photoperiods (Roenneberg & Foster, 1997). Hypocotyl elongation is such a physiological response that under diurnal growth conditions, displays rhythmic pattern with maximal elongation rate at the end of night (Nozue *et al*, 2007; de Montaigu *et al*, 2010).

Rhythmic hypocotyl growth under photoperiodic conditions is controlled by coordination between the circadian clock and light signaling networks (Nozue *et al*, 2007; Niwa *et al*, 2009; de Montaigu *et al*, 2010; Nomoto *et al*, 2012). Upon light exposure, phytochromes interact with a subset of basic helix–loop–helix (bHLH) phytochrome-interacting factors (PIFs) which trigger phosphorylation and degradation of PIF proteins resulting in a cascade of transcriptional changes to alter growth (Castillon *et al*, 2007; Jiao *et al*, 2007; Bae & Choi, 2008; Leivar & Quail, 2011; Pham *et al*, 2018). The circadian system integrates with PIF-dependent light signaling and gates maximal light responsiveness of hypocotyl elongation to specific times of day mainly through two mechanisms. The first is through the direct transcriptional regulation of *PIF4* and *PIF5* genes by the circadian clock which coincides with control of PIF protein accumulation by light (Nozue *et al*, 2007; Niwa *et al*, 2009; Nusinow *et al*, 2011; Nomoto *et al*, 2013; Li *et al*, 2020). The second mechanism relies on the temporal inhibition of the transcriptional activation activity of PIFs by clock proteins, such as TIMING OF CAB EXPRESSION 1 (TOC1) (Soy *et al*, 2016; Zhu *et al*, 2016), PSEUDO-RESPONSE REGULATORs (PRRs) (Martin *et al*, 2018;

1 Molecular Genetics, Ohio State University, Columbus, OH, USA
2 Memorial Sloan Kettering Cancer Center, Molecular Biology Program, New York, NY, USA
3 POSTECH, Division of Integrative Biosciences and Biotechnology, Pohang, South Korea
4 The Chinese Academy of Sciences, Institute of Botany, Beijing, China
5 RIKEN Center for Sustainable Resource Science (CSRS), Plant Proteomics Research Unit, Yokohama, Japan
6 Max Planck Institute for Plant Breeding Research, Protein Mass Spectrometry, Cologne, Germany
*Corresponding author. Tel: +1 614 292 2551; E-mail: somers.24@osu.edu

Zhang *et al*, 2020), and GIGANTEA (GI) (Nohales *et al*, 2019), which co-occupy the same genomic targets with PIF proteins.

Post-translational regulation of circadian systems has been widely studied in mammals, *Drosophila*, and *Neurospora* (Gallego & Virshup, 2007), and the role of phosphorylation in modulating transcriptional activity, subcellular localization, stability, and protein–protein interaction of clock proteins is well-documented (Saini *et al*, 2019; Brenna & Albrecht, 2020). Many plant clock proteins are also phosphorylated, and this modification is essential for their full biological function (Seo & Mas, 2014; Yan *et al*, 2021). CLOCK-ASSOCIATED 1 (CCA1), which comprises the morning loop with LATE ELONGATED HYPOCOTYL (LHY) in the autoregulatory feedback network of circadian clock, is phosphorylated by Casein kinase 2 (CK2), loss of which interferes with CCA1's transcriptional activity (Sugano *et al*, 1998; Daniel *et al*, 2004). Phosphorylation of PRR5 and TOC1 enhances interaction with the F-box protein ZEITLUPE (ZTL), facilitating their subsequent degradation (Fujiwara *et al*, 2008). TOC1/PRR3 phosphorylation-dependent interaction protects TOC1 from ZTL-dependent degradation, suggesting a complex interplay between phosphorylation and stability for these clock proteins. PRR5 enhances TOC1 phosphorylation and nuclear transport, implicating a phosphorylation-mediated mechanism of TOC1 nuclear import or subcellular re-distribution (Wang *et al*, 2010). However, direct evidence illustrating how TOC1's function is modulated by phosphorylation, which residues are phosphorylated and essential for TOC1 in sustaining circadian period and how it relates to gating of hypocotyl growth to photoperiods, is still lacking.

In this study, we identified 5 phosphorylation sites near the N-terminus of TOC1. Substitution of all 5 residues by alanine (5X) results in clock and developmental defects, similar to the *toc1-101* (hereafter *toc1*) mutant. Our genetic and biochemical evidence strongly suggests that TOC1 phosphorylation controls hypocotyl elongation through effects on circadian phase, protein stability, and chromatin residence of TOC1. TOC1 phosphorylation alters interactions with NUCLEAR FACTOR Y subunit C (NF-YC) and associations with HDA15 and PIF3, which together with NF-YB regulate downstream pre-dawn hypocotyl growth-related genes (PHGs) to precisely phase their expression to pre-dawn hours. PRR5 similarly interacts with NF-YB/C subunits and HDA15 and likely co-represses a subset of target genes together with TOC1. Collectively, our findings identify a molecular mechanism of how TOC1 phosphorylation controls photoperiodic hypocotyl elongation and highlight the essential role of post-translational regulation of TOC1 in synchronizing plant growth with cyclic environmental changes.

Results

Identification of TOC1 N-terminal phosphosites

In an effort to determine the role of phosphorylation in the function of TOC1, we performed mass spectrometry of the N-terminus (aa 1–242) when transiently co-expressed in *N. benthamiana* with PRR5, which visibly enhances TOC1 phosphorylation-dependent gel mobility (Wang *et al*, 2010). We identified 5 phosphorylated residues within and near the N-terminus pseudo-response receiver domain (PRR; Fig 1A). To determine whether mutations of the 5 phosphosites affect this enhancement, progressive alanine substitutions of the 5 residues were introduced and each was co-expressed with PRR5 in *N. benthamiana*.

In most lines, there was an increased relative abundance of upper (phosphorylated) vs. lower (unphosphorylated) forms of TOC1 in TOC1 wild type (TOC1WT), *T135A*, *S194A/S201A/T204A*, and *T135A/S194A/S201A/S204A* (Fig 1B). In contrast, an enhancement of the upper form of TOC1 was not observed in *S175A* and the quintuple mutant *T135A/S175A/S194A/S201A/S204A* (subsequently termed *5X*) (Fig 1B), indicating residue S175 is essential for TOC1 phosphorylation, as detected by mobility shift.

We next generated stable transgenic lines expressing GFP-tagged TOC1 WT, T135A, S175A, and 5X driven by the *TOC1* native promoter, and *TOC1 WT* and *5X* driven by the 35S promoter in the *toc1-101* background. TOC1 protein expression patterns in a time series (Appendix Fig S1A) and TOC1 protein expression levels at ZT1 and ZT13 (Appendix Fig S1B) were examined by Western blotting, and two independent lines for each transgene with similar expression level were selected for further characterization. Mobility shift assays revealed that 5X migrates faster than TOC1WT, indicating unphosphorylated 5X due to the phosphosite mutations (Fig 1C). Similar to 5X, the majority of S175A was in the unphosphorylated state, with a faint upper band. Pyrophosphatase treatment of TOC1 and T135A, but not 5X and S175A, was reverted by phosphatase inhibitors NaF/Na_3VO_4 (Fig 1C). These results suggest that mutation of all 5 phosphosites eliminates detectable TOC1 phosphorylation and S175 is the most essential residue for maintaining the phosphorylation state of TOC1.

S175A and 5X fail to fully rescue clock and developmental defects of *toc1*

To determine the *in vivo* significance of the 5 phosphosites, we next examined hypocotyl elongation in native promoter lines expressing WT, 5X, T135A, and S175A under constant red light. Wild-type *TOC1* and *T135A* fully rescued the long hypocotyl in *toc1-101* at all fluence rates tested, whereas *5X* and *S175A* failed to fully complement, especially at low fluence rates (Fig 2A–D). Overexpression of *TOC1* (*35S:TOC1*) strongly shortens hypocotyl length relative to WT, whereas *35S:5X* was much less effective (Fig 2E and F). Similar results were observed for both independent transgenic lines of each phospho-variant (Appendix Fig S2).

We further examined the hypocotyl length of the phosphosite mutants under short days (SD). Consistent with previous work (Soy *et al*, 2016), *toc1-101* hypocotyl is significantly longer than wild type, while TOC1 and T135A fully rescued the *toc1-101* phenotype. Similar to tests under red light, 5X and S175A also failed to complement under SD (Fig 3A and Appendix Fig S3A). *35S:TOC1* strikingly shortened hypocotyl length, while *35S:5X* displayed significant longer hypocotyl length than wild type, similar to *TOC1:5X* (Fig 3A and Appendix Fig S3A). Taken together, results under both growth conditions suggest the importance of these phosphorylations, especially at S175, in hypocotyl growth control by TOC1.

To examine the effects on circadian period, the *CCA1:LUC* reporter was crossed into the phosphosite mutant lines, and free-running period was measured. As expected, *toc1-101* showed a 19-h period and advanced phase compared to Col-0 with an approximately 24-h period (Fig 3B and C). *TOC1:TOC1* and *TOC1:T135A* more than rescued the short period and advanced phase, with both

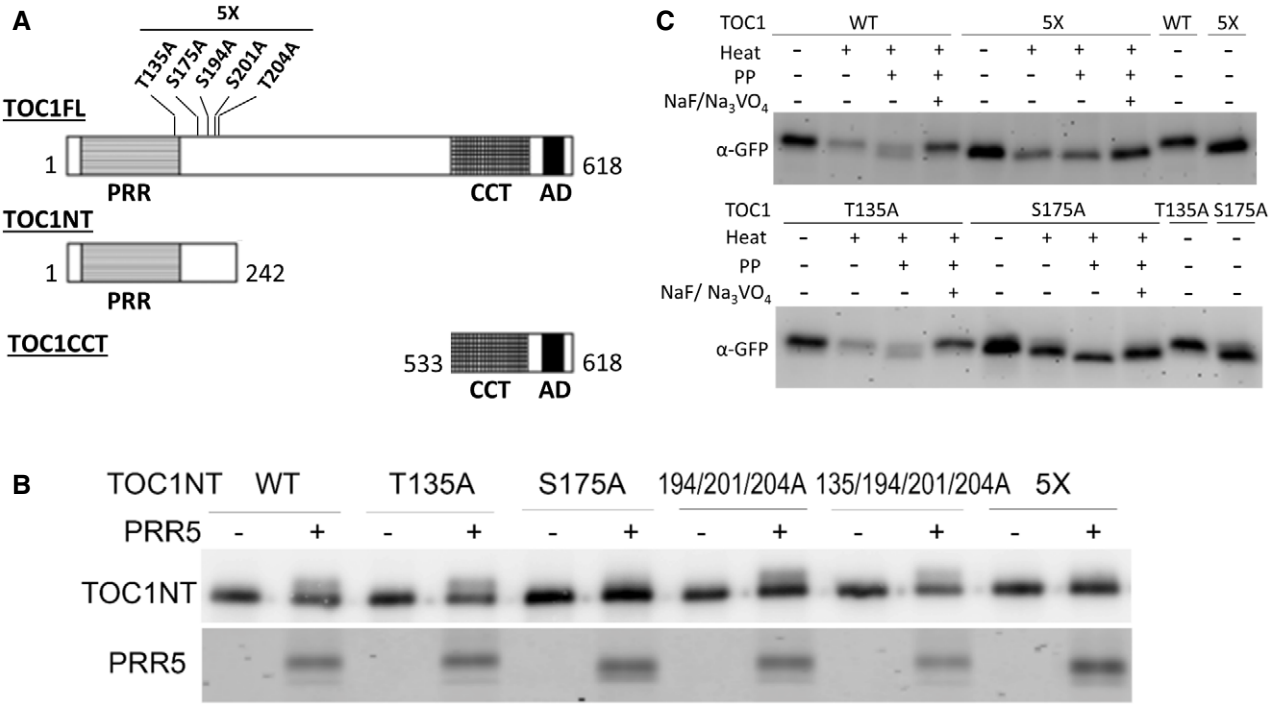

Figure 1. Phosphorylation-dependent protein mobility shift is eliminated or strongly reduced in *5X* and *S175A*.

A Schematic diagrams of full-length (FL), N-terminus (NT), and C-terminus CCT domain of TOC1 used in this manuscript. The 5 phosphorylated residues identified from our mass spectrometry were progressively substituted by alanine, and their positions are displayed on top of TOC1FL.

B Mutations in *S175* and *5X* attenuate PRR5's enhancement on TOC1 phosphorylation. Wild-type and phosphosite mutants of TOC1NT were transiently expressed with or without PRR5 in *N. benthamiana* leaves, and total proteins were extracted 3 days after infiltration.

C Phosphorylation of TOC1 is eliminated or largely reduced in *5X* and *S175A*. Total protein extracts (ZT13) from 10-day-old seedlings grown under 12-h/12-h light/dark cycles were subject to heat (30°C 20 min), pyrophosphatase (PP), and NaF/Na_3VO_4 (phosphatase inhibitors) treatments. TOC1-GFP at different phosphorylation states was separated by 8% SDS–PAGE (acrylamide:bisacrylamide 150:1) and subsequently detected by α-GFP.

Source data are available online for this figure.

showing a slightly longer period, likely due to slightly higher than endogenous levels of TOC1 expression coming from the transgenes. In contrast, the period of *TOC1:5X* and *TOC1:S175A* was intermediate between *toc1-101* and *TOC1:TOC1*; 2 h shorter than Col-0 and with an earlier phase (Fig 3B–D and Appendix Fig S3B). Overexpression of *TOC1(35S:TOC1)* significantly lengthened period to more than 29 h and delayed the phase of *CCA1:LUC*. *35S:5X* displayed a much shorter period and more advanced phase than Col-0, statistically similar to *TOC1:5X* and *TOC1:S175A* (Fig 3B and E, and Appendix Fig S3B). The much longer period of *35S:TOC1* line #2 than #1 likely results from the higher TOC1 protein levels in this line (Appendix Fig S1B).

Flowering time was also examined in these same native promoter lines grown under SD. TOC1 and T135A fully rescued the early flowering phenotype of *toc1-101* whereas 5X and S175A did not (Appendix Fig S3C). Taken together, these results suggest that phosphorylation of the five residues in TOC1, particularly S175, is essential for its full function in controlling circadian period and development.

Phospho-mutants de-repress PHGs

TOC1 down-regulates PHGs, such as *PIL1*, *AT5G02580*, and *CDF5*, by repressing the transcriptional activity of PIF3 (Soy *et al*, 2016; Martin *et al*, 2018). The longer hypocotyl in the *5X* and *S175A* lines could result from increased expression of these genes. We further investigated the expression level of *PIL1*, *AT5G02580*, and *CDF5* during the pre-dawn phase in Col-0, *toc1-101*, *TOC1:TOC1*, and *TOC1:5X*. Consistent with previous results, the expression of the tested PHGs was strongly increased from ZT15 to ZT23 with the peak expression near the end of night. Loss of TOC1 function in *toc1-101* resulted in an even stronger increased expression of these genes (Fig 4A–C). *TOC1:TOC1* rescued the high expression of all three genes in *toc1-101* to WT levels whereas *TOC1:5X* failed to fully repress their expression (Fig 4D–F). *T135A* rescued *PIL1*, *AT5G02580*, and *CDF5* gene expression to WT levels, whereas *S175A* was unable to fully complement *CDF5* expression at ZT18 (Fig EV1). These results indicate that the longer hypocotyl length of *TOC1:5X* and *TOC1:S175A* is at least partially due to de-repression of PHGs, and *TOC1:S175A* may affect a smaller set of genes than *TOC1:5X*.

TOC1 phospho-mutations weaken PIF3 interaction and chromatin residence

De-repression of the PHGs in the *5X* line may result from a reduced physical interaction between TOC1 5X and PIF3. We then examined the effect of TOC1 phosphorylation on its interaction with PIF3 by

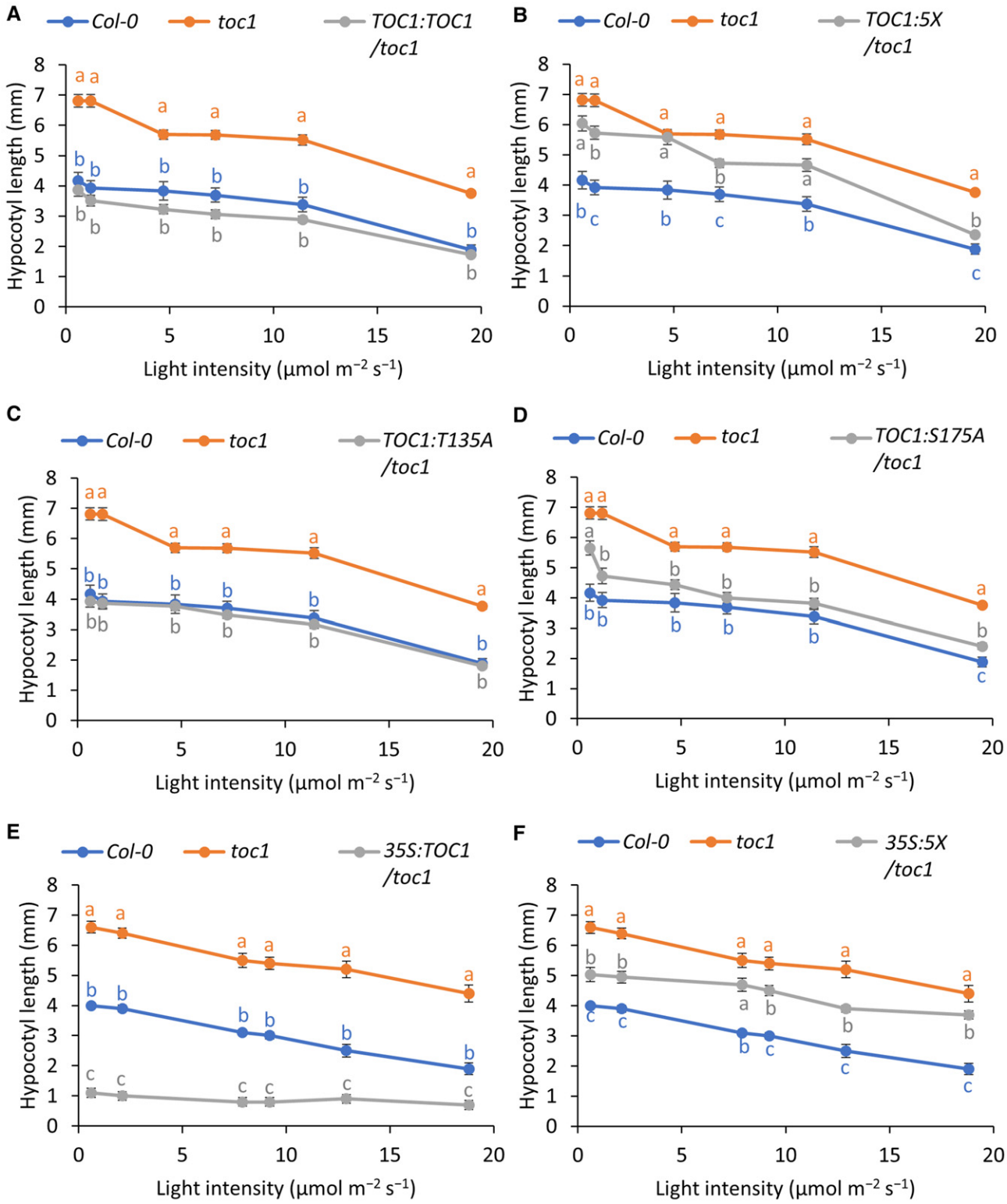

Figure 2. *5X* and *S175A* fail to fully rescue the hypocotyl phenotype displayed in *toc1-101*.

A–F Shown are hypocotyl lengths of cRL-grown 4-day-old seedlings of *toc1* complemented with wild-type *TOC1* (A), *5X* (B), *T135A* (C), and *S175A* (D) driven by *TOC1* native promoter and wild-type TOC1 (E), *5X* (F) driven by 35S promoter at sequential fluence rates. Different letters indicate statistically significant differences between genotypes ($P < 0.01$, one-way ANOVA followed by Tukey–Kramer HSD test), and error bars indicate SEM. Data are representative of three biological trials with similar results.

Source data are available online for this figure.

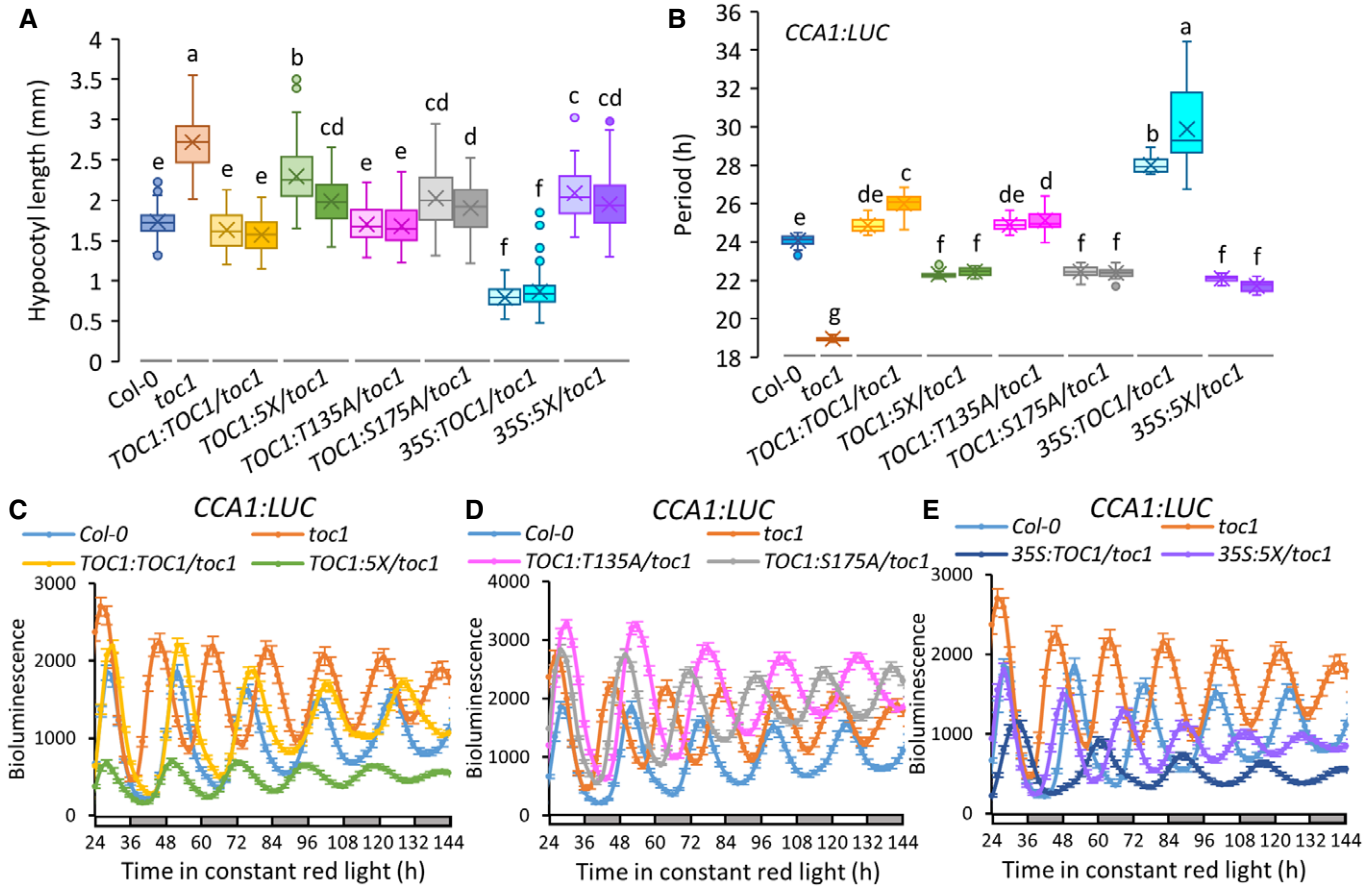

Figure 3. *5X* and *S175A* incompletely rescue *toc1-101* defects in period length, expression phase, and hypocotyl growth.

A, B Hypocotyl lengths under SD (A) and free-running period (B) of Col-0, *toc1-101* and independent native and 35S promoter lines expressing wild-type TOC1 and each phosphosite mutant. The middle line of the box represents the median, the x in the box represents the mean. The bottom line and the top line of the box represent 1st and 3rd quartile, respectively. The whiskers extend from the ends of the box to the minimum value and maximum value.

C–E Average *CCA1:LUC* bioluminescence traces of indicated plant lines.

Data information: For A, seedlings were grown under white light and SD (8-h/16-h L/D) for 3 days. 100 seedlings from 4 independent trials were averaged. For B–E, 18–27 seedlings per line were entrained in 12-h/12-h light/dark cycles for 7 days then transferred to constant red light at ZT2 for image acquisition at 2-h intervals for 1 week. White and gray regions indicate subjective light and dark periods. Data are representative of at least two independent trials with similar results. Different letters indicate statistically significant differences in hypocotyl length and period between genotypes ($P < 0.01$, one-way ANOVA followed by Tukey–Kramer HSD test).
Source data are available online for this figure.

transiently co-expressing PIF3-TAP with either TOC1-GFP or 5X-GFP in *N. benthamiana*. Wild-type TOC1 co-immunoprecipitated (Co-IPed) with PIF3, but interaction between PIF3 and 5X was only 60% of WT (Fig 5A and B and Appendix Fig S4A), suggesting TOC1 phosphorylation is important for PIF3 binding. However, further tests with TOC1NT (aa 1–242), which contains the five phosphorylation sites, found that neither WT nor 5X NT Co-IPed with PIF3 (Appendix Fig S4A). This suggests that despite the binding enhancement by N-terminal phosphorylation, additional domains of TOC1 are needed for PIF3 interaction.

We next tested whether the diminished association between 5X and PIF3 altered enrichment of TOC1 at three PIF3 target promoters, *PIL1*, *AT5G02580*, and *CDF5*. ChIP-qPCR showed both TOC1 and 5X were significantly enriched at the promoter of all three genes. However, 5X had 40–50% lower abundance at these promoter regions than TOC1 WT (Fig 5C), suggesting that TOC1 phosphorylation promotes chromatin residence at these gene promoters.

As PIF proteins have been reported to anchor PRR association to target DNA (Zhang *et al*, 2020), we next crossed *TOC1:TOC1-GFP* into *pif3/4/5 toc1* quadruple mutant background and assessed whether PIFs facilitate TOC1 binding to the promoter of *PIL1*, *AT5G02580*, and *CDF5* by ChIP-qPCR. This could explain the reduced chromatin presence of 5X through the weaker interaction with PIF3. We ensured similar protein abundance between different mutant backgrounds at tissue harvest time (Appendix Fig S4B). Results showed significant enrichment of TOC1 at *PIL1*, *AT5G02580*, and *CDF5* promoters, largely independent of PIF3, PIF4, and PIF5 (Fig 5D), similar to previous reports (Soy *et al*, 2016). However, we cannot exclude the possibility that other PIF proteins may recruit TOC1 to the target promoters (Li *et al*, 2020; Zhang *et al*, 2020). Taken together, these data suggest two functional defects of the

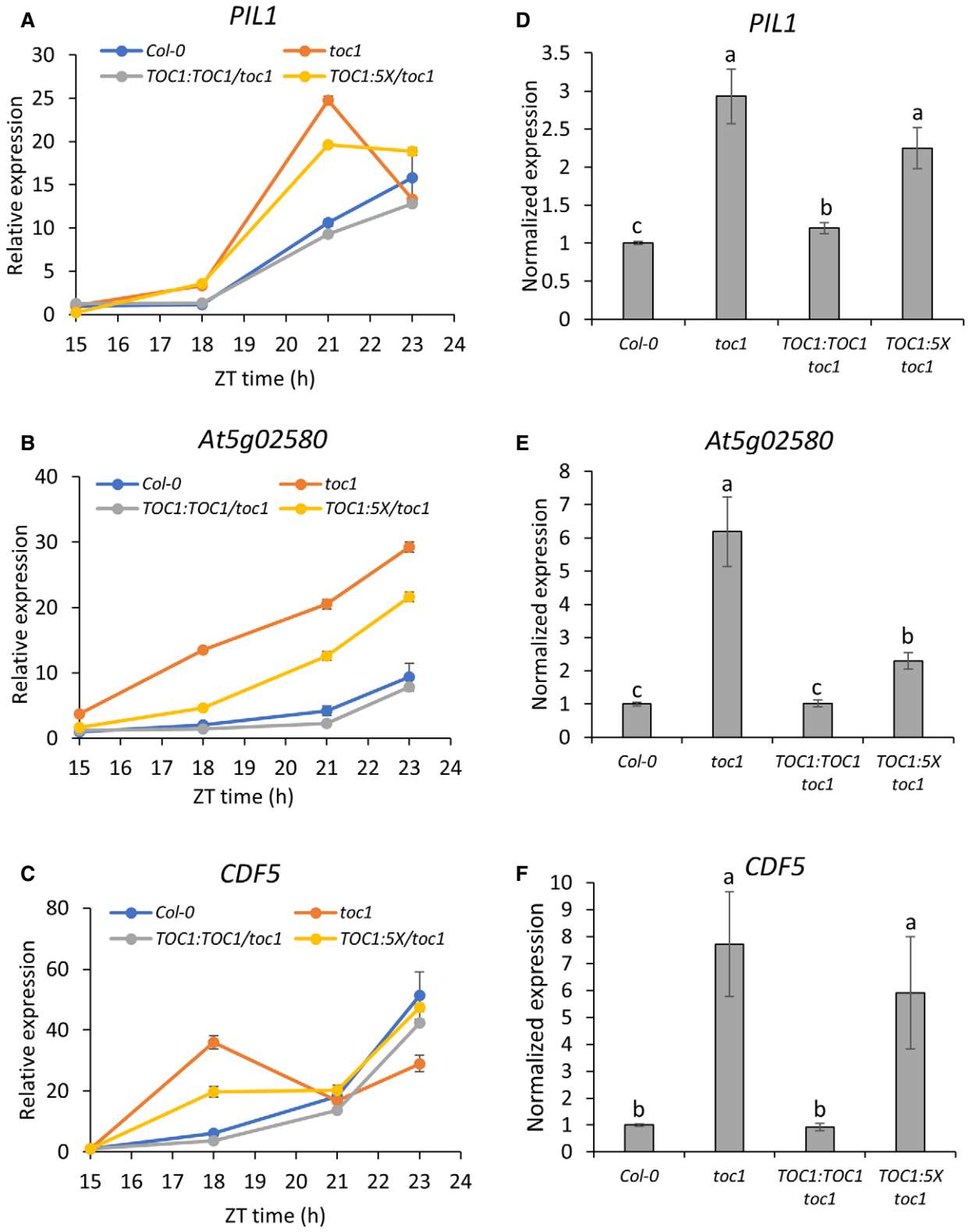

Figure 4. Mutations in *5X* de-repress the pre-dawn hypocotyl growth-related genes (PHGs).

A–C *PIL1*, *AT5G02580*, and *CDF5* expression pattern in 3-d-old SD-grown seedlings from indicated plant lines at night. Data are representative of 3 biological trials.

D–F Expression of *PIL1*, *AT5G02580*, and *CDF5* in 3-d-old SD-grown seedlings at ZT18. 5 biological trials were averaged, and error bars indicate SEM. Different letters denote statistically significant differences based on Wilcoxon test ($P < 0.05$).

Source data are available online for this figure.

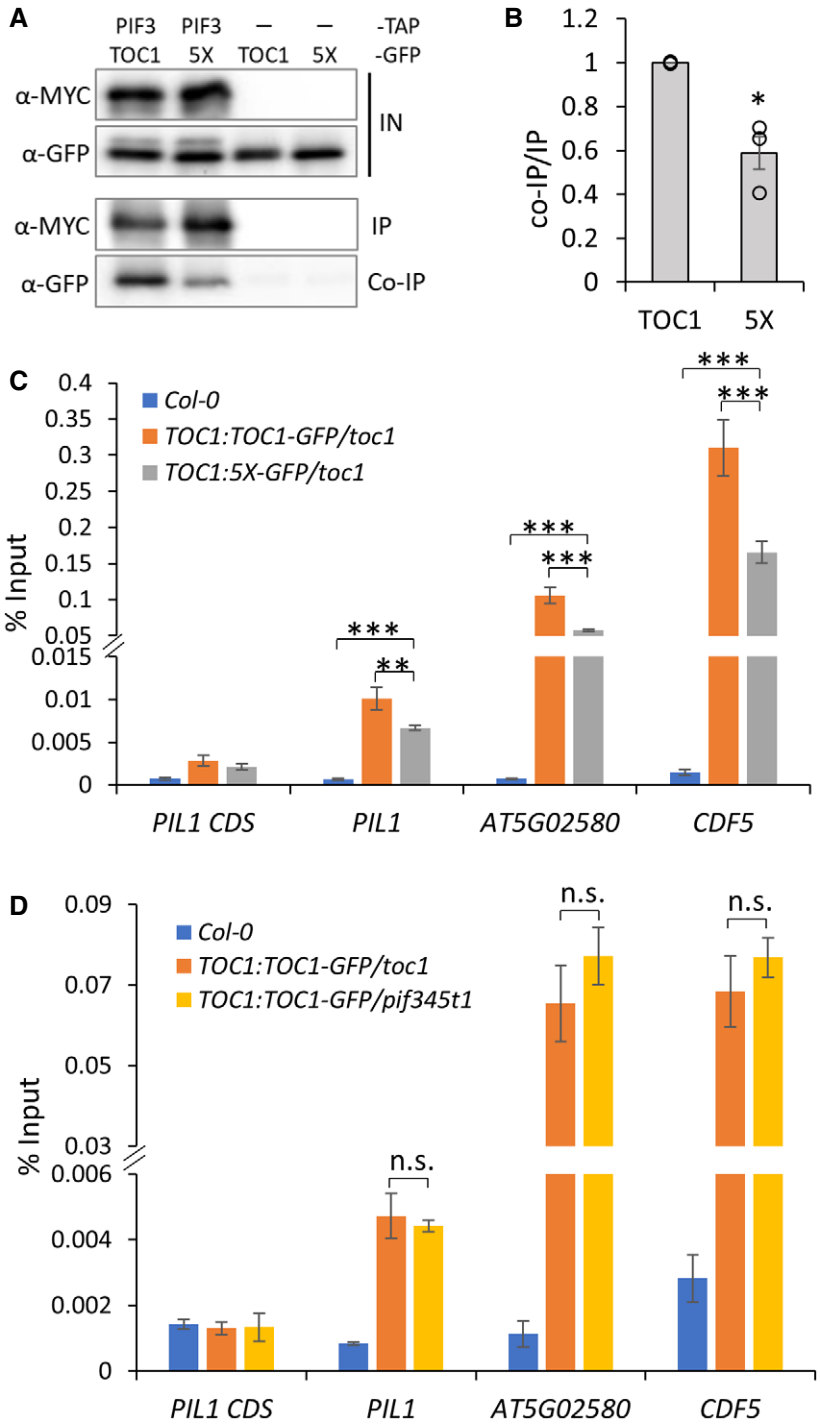

Figure 5. 5X interacts more poorly with PIF3 and is present to a lesser extent at PIF3 target promoters.

A Co-IP of PIF3-TAP with TOC1-GFP vs. 5X-GFP in *N. benthamiana*. Protein extracts were immunoprecipitated by IgG resins followed by HRV-3C protease digestion. PIF3 and TOC1 were detected by anti-MYC and anti-GFP, respectively.

B Quantification of protein interaction in A. Results from 3 independent trials were averaged. Error bars indicate SEM, and asterisks indicate significant difference (*$P < 0.05$, Student's *t*-test).

C ChIP-qPCR of TOC1 binding to promoters of pre-dawn-phased PIF3 target genes at ZT14 in Col-0, native promoter *TOC1* and *5X* lines.

D ChIP-qPCR of the chromatin residence of TOC1-GFP at target promoters in *toc1* and *pif3/4/5 toc1* (*pif345t1*) mutant backgrounds.

Data information: For C and D, 3-d-old SD-grown seedlings were harvested at ZT14, and TOC1-GFP was immunoprecipitated by α-GFP and magnetic protein G beads. Data from 3 independent trials were averaged, and error bars indicate SEM. Asterisks indicate significant differences (**$P < 0.001$, ***$P < 0.0001$, Student's *t*-test), n.s. = not significant.
Source data are available online for this figure.

unphosphorylated 5X are a diminished interaction with PIF3, and independently, a reduction in chromatin presence at key PHGs.

Early phasing of S175A and 5X reduces TOC1 pre-dawn accumulation

The phasing of TOC1 expression is important to its role in both circadian and diurnal gene regulation, so we further tested TOC1 protein accumulation in native promoter *TOC1/5X/T135A/S175A* lines under SD. Quantitation of TOC1 abundance at sequential time points showed similar TOC1 protein accumulation patterns for wild-type TOC1 and *T135A*. In both cases, TOC1 levels increased during the photoperiod, attaining maximum expression post-dusk (ZT8-14), with a gradual decrease to the end of night (Figs 6A and EV2A).

In contrast, *5X* and *S175A* displayed a more rapid increase in TOC1 accumulation from ZT2 to ZT8, peaking at ZT8, and diminishing more quickly than *TOC1* and *T135A* at night (Figs 6A and EV2A). Two independent lines of each phosphosite mutant show similar patterns of TOC1 protein accumulation under SD (Figs 6A and EV2A). The *TOC1:TOC1* line #2 has slightly stronger expression and shows a more striking phase shift relative to *5X* and *S175A* (Fig EV2A). Consistent with slightly greater protein abundance, *TOC1:TOC1* line #2 exhibits a shorter hypocotyl length and longer

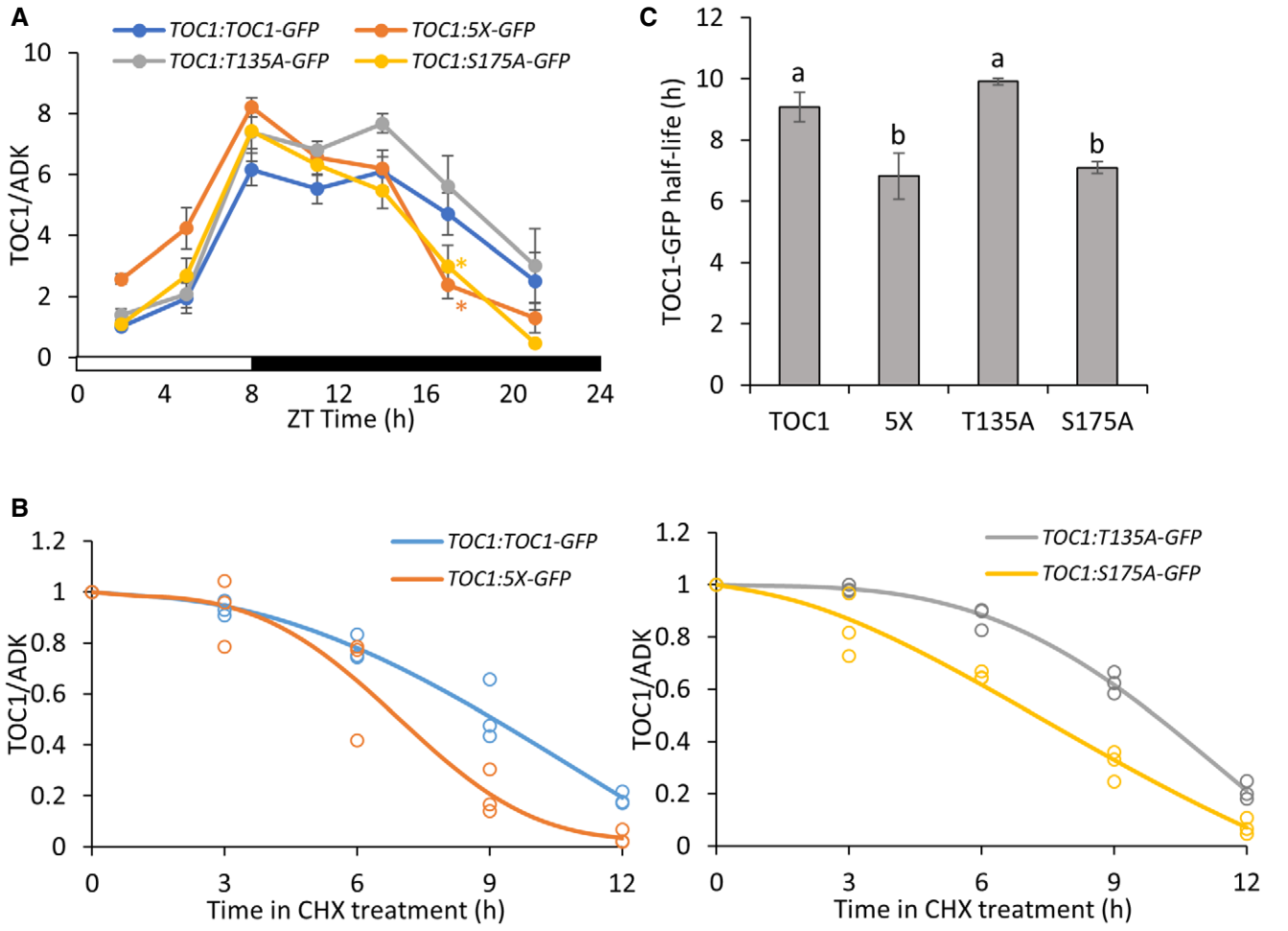

Figure 6. TOC1 phospho-mutants show early-phased protein expression and reduced stability.

A TOC1 protein expression pattern in 3-d-old seedlings in native promoter *TOC1/5X/T135A/S175A* lines grown in SD. White and black regions indicate light and dark periods. Data from 3 independent trials were averaged; error bars indicate SEM. Statistical analyses were performed by Student's *t*-test. Asterisks indicate significant differences between TOC1 wild-type and its phosphosite mutants (*$P < 0.05$).

B Measurement of TOC1-GFP protein turnover in *TOC1*, *5X*, *T135A*, *S175A* native promoter lines by cycloheximide (CHX) treatment. 10-d-old seedlings grown in 12-h/12-h light/dark cycles were subject to cycloheximide (CHX) or ethanol (Mock) treatment for indicated time length. Data from 3 independent trials were fitted to non-linear Weibull regression curves.

C Estimates of TOC1-GFP protein half-life in B. Error bars indicate SEM, statistical analyses were performed with Student's *t*-test, and different letters indicate significant differences ($P < 0.05$). Data from 3 independent trials were averaged.

Data information: For A and B, TOC1 protein was detected by α-GFP, and ADK was used as loading control. TOC1/ADK ratio was calculated by the intensities of TOC1-GFP bands normalized by the intensities of ADK bands using ImageJ.
Source data are available online for this figure.

period than Col-0 and *TOC1:TOC1* line #1 (Appendix Fig S2A and S3B and Fig 3B). This phase advance of *5X* and *S175A*, which arises from the shorter period in these two backgrounds (Fig 3B), reduces the accumulation of two phospho-variants at night, diminishing the amount of time they are available for *PIF3* repression. This results in greater expression of PHGs (Figs 4 and EV1; *PIL1*, *AT5G02580*, and *CDF5*) and demonstrates the importance of TOC1 phasing in controlling gene expression.

TOC1 phospho-mutants diminish protein stability and dimerization but not nuclear import

TOC1 phosphorylation-mediated interaction with PRR3 has been implicated in regulating its stability (Para *et al*, 2007; Fujiwara *et al*, 2008), so we next sought to investigate whether the phosphosite mutants alter TOC1 turnover. TOC1 degradation rates in cycloheximide (CHX) treated *TOC1/5X/T135A/S175A* seedlings were nearly identical between wild-type *TOC1* and *T135A* lines, whereas *5X* and *S175A* plants showed significantly more rapid turnover (Fig 6B and C). These results suggest TOC1 protein stability is enhanced by phosphorylation.

TOC1 stability and phosphorylation are promoted by heterodimerization with PRR5 (Wang *et al*, 2010), but TOC1 homodimerization has not been reported. We tested TOC1-TOC1 interaction by yeast two-hybrid (Y2H) and Co-IP for both WT and 5X proteins after first establishing that TOC1 is phosphorylated in yeast (Appendix Fig S5A). Y2H assays showed reduced interaction between WT and 5X proteins that was diminished further when the 5X-5X pairing was tested (Appendix Fig S5B). Similar results were seen *in planta* with a 20–25% reduction in interaction when at least one partner was the 5X phospho-mutant (Appendix Fig S5C). These findings strongly suggest that N-terminal phosphorylation facilitates TOC1 homodimerization.

Studies in other circadian systems have suggested that phosphorylation often promotes nuclear import (Blau, 2008; Diernfellner *et al*, 2009), and in plant system, PRR5 has been found to enhance TOC1 phosphorylation and nuclear accumulation (Wang *et al*, 2010). When nuclear and cytosolic fractions of wild-type TOC1 and 5X proteins were prepared, we found no differences in protein partitioning (Fig EV2B), indicating that the phosphorylation state of TOC1 does not alter its nucleocytoplasmic distribution.

Phosphorylation likely promotes TOC1-NF-YB/C interactions

NUCLEAR FACTOR Y (NF-Y) transcription factors are trimeric protein complexes composed of NF-YA, NF-YB, and NF-YC subunits. Loss of *NF-YC3/4/9* results in greater hypocotyl length by derepression of hypocotyl growth-related genes (Myers *et al*, 2016; Tang *et al*, 2017) linking NF-Y complexes to hypocotyl growth control. Therefore, we next tested whether TOC1 functions *in vivo* with NF-YB/C dimers and assessed the role of TOC1 phosphorylation in this relationship.

Y2H assays between TOC1 and NF-YB/C identified positive interactions between TOC1 and NF-YC3/4/9 but not with NF-YB2/3, and similar results were also found for 5X (Fig 7A and Appendix Fig S6F). *In planta* interaction tests in *N. benthamiana* showed little or no NF-YB2/3 Co-IPed with TOC1 or 5X, consistent with the Y2H results (Appendix Fig S6A). TOC1 and 5X weakly interact with NF-YC3/4/9 alone (Fig 7B and Appendix Fig S6B–D). However, the presence of NF-YB2/3 strongly enhanced TOC1 interaction with NF-YC3/4/9 by threefold to fourfold, and NF-YB now precipitate together with NF-YC and TOC1 (Fig 7B and Appendix Fig S6B–D). Similar results were found for all combinations of NF-YB2/3 and NF-YC3/4/9 in our Co-IP assays and are consistent with a recent report of *in vitro* interactions between TOC1 and NF-YB2/C3 (Shen *et al*, 2020) and previous Y2H tests with *Brachypodium* NF-YC orthologs (Cao *et al*, 2011).

Furthermore, the interaction between 5X and NF-YC3 and NF-YC9 (in the presence of B2 or B3) was reduced 30% compared with TOC1 WT, whereas 5X interaction with NF-YC4 was similar to TOC1 WT (Fig 7B and Appendix Fig S6B–D). These results strongly suggest that TOC1 forms a trimeric complex with NF-YB/C dimers *in vivo*, and phosphorylation promotes the physical interaction between TOC1 and some NF-YB/C dimers.

We next tested whether the N-terminus (NT) of TOC1 and 5X is responsible for NF-YB/C interactions. None of the tested NF-YC subunits significantly Co-IPed with the TOC1 or 5X NT even in the presence of NF-YB (Appendix Fig S7A and B). As *in vitro* assays show that the CCT domain of TOC1 is essential for interactions with NF-YB/C (Shen *et al*, 2020), we next examined whether the TOC1ΔCCT (1–527 aa) or the TOC1 CCT domain alone (533–574 aa) interacts with NF-YB/C. Compared to full-length TOC1, similar amounts of each NF-YC3/9 were Co-IPed with TOC1ΔCCT, but enhancement by NF-YB was absent for the deletion (Fig EV3A and B). In contrast, while neither NF-YC3 nor NF-YC9 showed a detectable interaction with the CCT domain, addition of NF-YB2 increased interaction between CCT and NF-YC proteins (Fig EV3A and B), indicating the CCT domain is important for the NF-YB2-mediated enhancement of the interaction between TOC1 and NF-YC. While previous findings reported that deletion of the CCT domain abolishes *in vitro* interaction between TOC1 and NF-YB2/C3 (Shen *et al*, 2020), our detection of protein interactions between TOC1ΔCCT and NF-YC3/C9 might be facilitated by TOC1ΔCCT dimerization with endogenous NbTOC1 (and possibly other NbPRRs) in our *in vivo N. benthamiana* system. Taken together, these results suggest that neither the NT nor the CT of TOC1 alone are sufficient for the optimal interaction with NF-YB/C.

We next examined chromatin residence of WT and 5X TOC1 in the *nf-yc3/4/9* triple mutant after first determining that TOC1 protein expression is not altered in the *nf-yc3/4/9* background (Appendix Fig S6E). The absence of NF-YC3/4/9 resulted in ~50% reduced residence of TOC1 at the promoter of PHGs (*PIL1*, *AT5G02580*, and *CDF5*), and 5X exhibited significantly decreased chromatin binding only at *CDF5* (Fig 7C). These results indicate that NF-YC proteins enhance TOC1 residence at these target genes. While N-terminal phosphorylation of TOC1 is important for NF-YC3 and C9 interaction (Fig 7B), the absence of NF-YC3/4/9 has little added effect in the diminished 5X chromatin presence, likely due to the already strong loss of TOC1 residence in that mutant background.

TOC1-HDA15 interaction is destabilized by phospho-mutations

NF-YC subunits can recruit HDA15 to the promoter of hypocotyl growth-related genes and repress their expression through histone deacetylation (Tang *et al*, 2017). Having established the formation

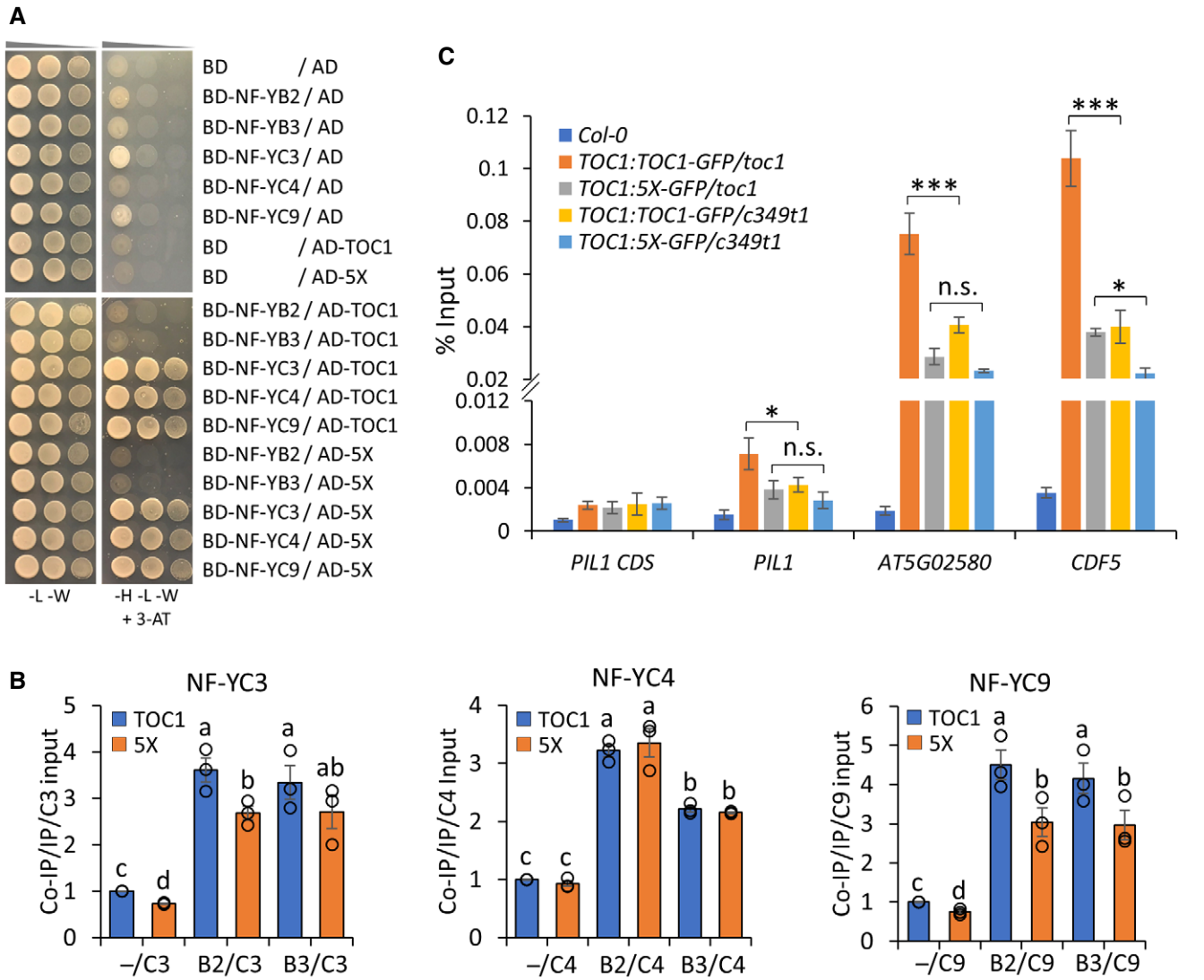

Figure 7. NF-YB/C forms trimeric complex with TOC1 and stabilizes TOC1 at target promoters.

A Yeast two-hybrid (Y2H) assay of interactions between the Gal4 DNA-binding domain BD-NF-YB2/3, BD-NF-YC3/4/9, and Gal4 activation domain AD-TOC1/5X fusions. Yeast growth shown on leucine-, tryptophan-deficient plate indicates successful plasmid transformation, and yeast growth shown on leucine-, tryptophan-, histidine-deficient and 3-AT plate indicates positive protein interactions.

B Quantification of interactions between TOC1/5X-TAP and NF-YC proteins in the presence or absence of NF-YB subunits. Proteins were transiently expressed in *N. benthamiana*. TOC1/5X was immunoprecipitated with IgG resins followed by HRV-3C protease digestion. TOC1/5X and NF-YB/C were detected by α-MYC and α-HA, respectively. Protein band intensity was measured by ImageJ, and interactions were exhibited as ratio of co-immunoprecipitated NF-YC to immunoprecipitated TOC1/5X to NF-YC input. Results from 3 independent trials were averaged. Error bars indicate SEM, and different letters denote significant differences ($P < 0.05$, Student's *t*-test).

C ChIP-qPCR of TOC1-GFP and 5X-GFP's residence at target promoters in *toc1* and *nf-yc3/4/9 toc1* (*c349t1*) mutants. 3-d-old SD-grown seedlings were harvested at ZT14, and TOC1 and 5X were immunoprecipitated by α-GFP and magnetic protein G beads. Data from 3 independent trials were averaged. Error bars indicate SEM, and asterisks indicate significant differences (*$P < 0.05$, ***$P < 0.0001$, Student's *t*-test), n.s. = not significant.

Source data are available online for this figure.

of a trimeric protein complex of TOC1 with NF-YB/C, we next examined the interaction between TOC1 and HDA15.

In Co-IP assays, both TOC1-GFP and 5X-GFP successfully Co-IPed with HDA15-TAP (Fig 8A), although 5X interacts 34% more poorly with HDA15 than WT TOC1 (Fig 8B), suggesting phosphorylation of TOC1 stabilizes the interaction. We next sought to understand the genetic relationship between TOC1, NF-YC, and HDA15 through double and quadruple mutant analysis. Both *toc1-101* single and *nf-yc3/4/9* triple mutants showed significant longer hypocotyls compared with Col-0, and the quadruple mutant displayed synergistically greater hypocotyl elongation than *toc1-101* and *nf-yc3/4/9* under SD (Fig 8C). This result suggests other PRR proteins (e.g., PRR5) may also act to anchor NF-YCs to target promoters in the absence of TOC1, and conversely, that additional NF-YC proteins

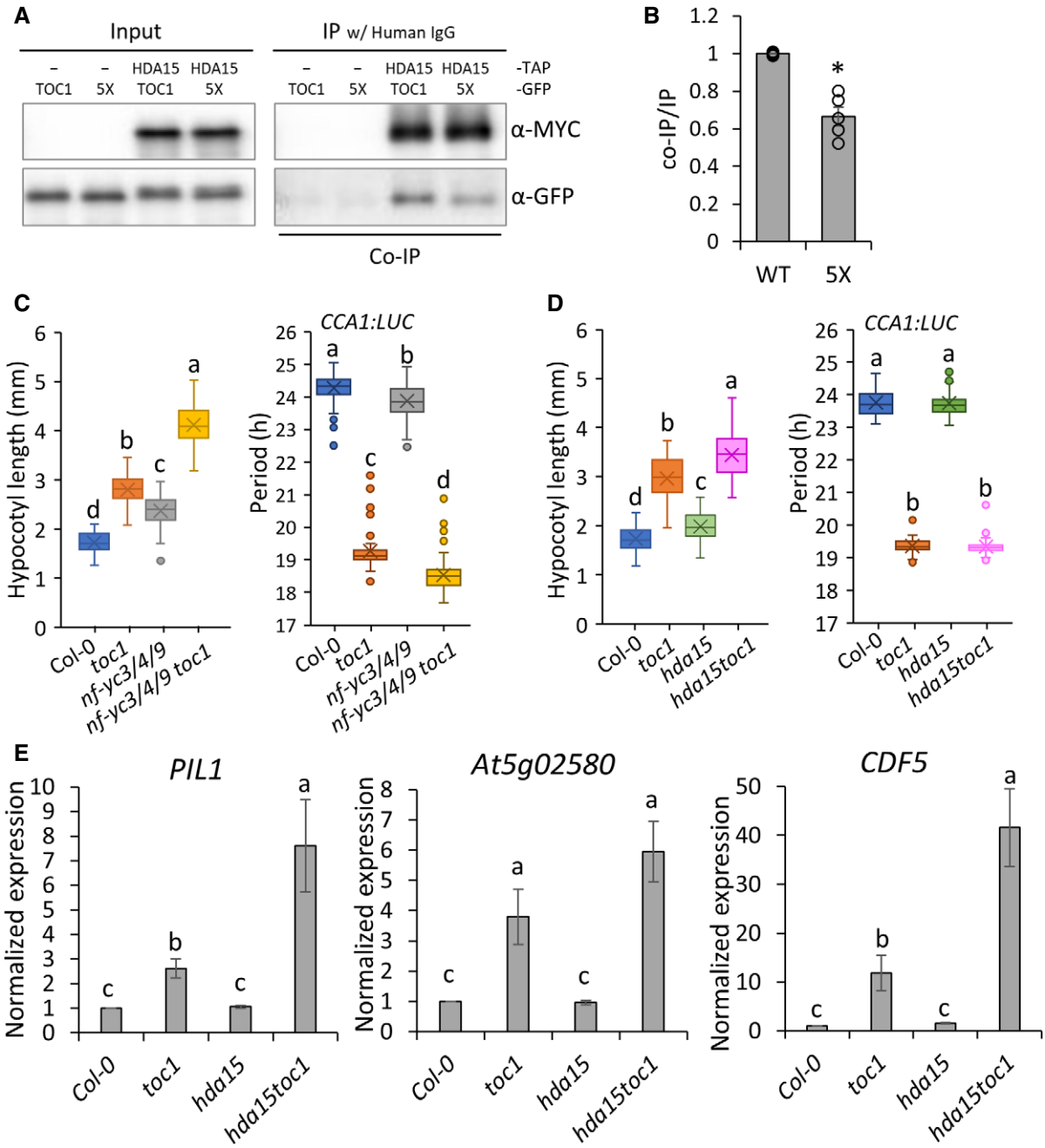

Figure 8. NF-YB/C and HDA15 repress downstream hypocotyl genes together with TOC1.

A Co-IP assay of HDA15-TAP with TOC1-GFP and 5X-GFP in *N. benthamiana*. HDA15-TAP was immunoprecipitated with IgG resins and digested by HRV-3C protease. HDA15 and TOC1 were detected by α-MYC and α-GFP, respectively.

B Quantification of the interaction strength in A. Results from 5 independent trials were averaged. Error bar indicates SEM, and asterisk indicates significant difference (*$P < 0.05$, Student's *t*-test).

C, D Hypocotyl lengths and free-running periods of indicated plants lines. Data of ~75 plants from 3 independent experiments were averaged, and different letters indicate statistically significant differences ($P < 0.01$, one-way ANOVA followed by Tukey–Kramer HSD test). The middle line of the box represents the median, and the x in the box represents the mean. The bottom line and the top line of the box represent 1st and 3rd quartiles, respectively. The whiskers extend from the ends of the box to the minimum value and maximum value.

E Expression of *PIL1*, *AT5G02580*, and *CDF5* in 3-d-old SD-grown seedlings at ZT18. Data from 3 independent experiments were averaged. Error bars indicate SEM. Different letters denote statistically significant differences based on Wilcoxon test ($P < 0.05$).

Source data are available online for this figure.

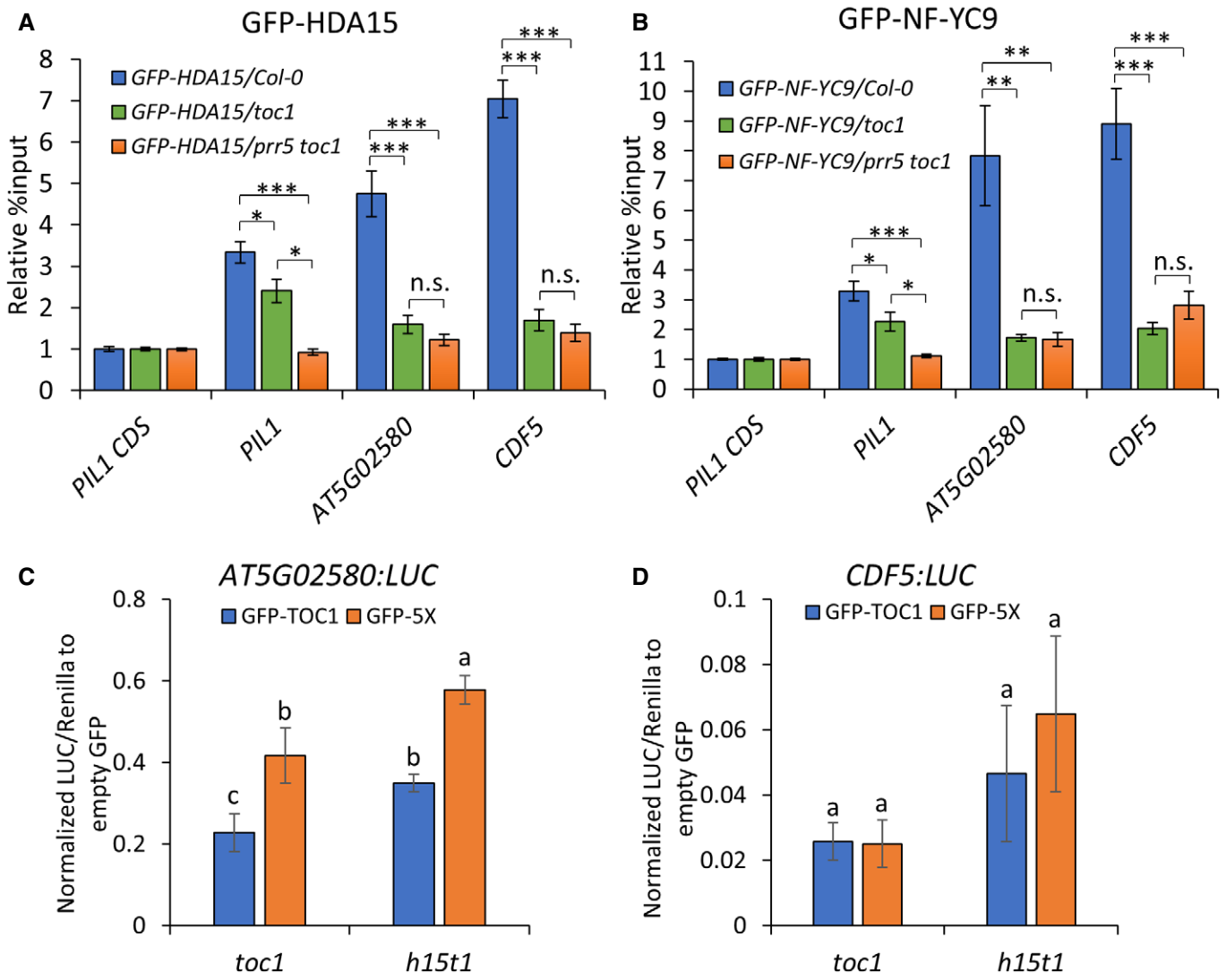

Figure 9. TOC1 and PRR5 anchor HDA15 and NF-YC9 to target promoters.

A, B ChIP-qPCR assay of HDA15's (A) and NF-YC9's (B) residence at target promoters in the presence or absence of TOC1 and PRR5. *35S::GFP-HDA15* and *35S::GFP-NF-YC9* were transiently expressed in protoplasts isolated from Col-0, *toc1* single, and *prr5 toc1* double mutant grown in SD condition. Results were normalized by % input of *PIL1* coding region (*PIL1 CDS*). Data from at least 3 independent experiments were averaged, and error bars indicate SEM. Asterisks indicate significant differences (*$P < 0.05$, **$P < 0.001$, ***$P < 0.0001$, Student's *t*-test).

C, D Dual-luciferase assay of the repression activity of GFP-TOC1 and GFP-5X on promoter of *AT5G02580* (C) and *CDF5* (D) in protoplasts of *toc1* and *hda15toc1* (*h15t1*) mutants. *AT5G02580:LUC*, *CDF5:LUC* reporters and the effectors (empty GFP, GFP-TOC1, and GFP-5X) were co-transfected to *toc1* and *hda15 toc1* protoplasts with *35S:Renilla-LUC* as an internal control. Data are means ± SEM ($n = 5$ biological trials) relative to empty GFP which is set as 1. Different letters indicate statistically significant differences (Student's *t*-test, $P < 0.05$).

Source data are available online for this figure.

(e.g., NF-YC1; Tang *et al*, 2017) may contribute to the NF-TOC1 complex. These mutant combinations also have additive effects on circadian period (Fig 8C), suggesting similar complexes control clock gene expression.

The *hda15-1* single mutant had slightly longer hypocotyls than Col-0, while the effect of a double mutant of *toc1* and *hda15-1* is additive (Fig 8D). Similar to the above, the absence of simple epistasis between the *toc1* and *hda15* mutants suggests additional PRR and HDA family components controlling hypocotyl length. In contrast, *hda15* has no detectable effect on circadian period (Fig 8D).

We then examined the expression of *PIL1*, *AT5G02580*, and *CDF5* in these new plant lines. While the absence of HDA15 alone has no effect on the expression of these genes, loss of TOC1 and HDA15 together synergistically increased their expression in most cases (Fig 8E).

To further test whether HDA15 affects chromatin binding of TOC1, we performed ChIP-qPCR of native promoter *TOC1/5X* lines

in *toc1* single vs. *hda15 toc1* double mutant background. As expected, 5X showed significantly reduced chromatin residence compared with wild-type TOC1 in both mutant backgrounds (Appendix Fig S8). However, loss of HDA15 only altered the enrichment of TOC1 to the *PIL1* promoter.

These results indicate that TOC1, NF-YC, and HDA15 function together in a protein complex to control expression of a subset of hypocotyl growth-related genes but may also have divergent roles and interact with different proteins to regulate different target gene subsets.

TOC1 and PRR5 recruit HDA15 and NF-YC9 to TOC1 target promoters

To further determine the biological significance of TOC1 interactions with NF-YB/C and HDA15, we transiently expressed GFP-HDA15 (Fig 9A) or GFP-NF-YC9 (Fig 9B) in protoplasts isolated from three different genotypes (Col-0, *toc1-101*, and *prr5 toc1*) and performed ChIP-qPCR. In WT, GFP-HDA15 and GFP-NF-YC9 were significantly enriched at *PIL1*, *AT5G02580*, and *CDF5* promoters (Fig 9A and B). The absence of TOC1 strikingly diminished the chromatin occupancy of HDA15 and NF-YC9 at *PIL1*, *AT5G02580*, and *CDF5*, indicating the importance of TOC1 in helping anchor both proteins to promoters.

PRR5 is a closely related homolog of TOC1 and has overlapping functions in regulating the clock and hypocotyl elongation (Ito *et al*, 2007, 2008; Fujiwara *et al*, 2008; Li *et al*, 2020). We thus performed the same assays in *prr5 toc1* protoplasts. In the double mutant HDA15 and NF-YC9 residence was further reduced at the *PIL1* promoter but there was little additional effect at *AT5G02580* and *CDF5* promoters (Fig 9A and B). Variations in non-specific chromatin binding of GFP were found in protoplasts of different genetic backgrounds, but no evident enrichment of GFP alone was observed at target promoters (Appendix Fig S9A). Balanced protein expression in protoplasts from different genetic backgrounds was validated by Western blot (Appendix Fig S9B) to exclude the possibility that the altered chromatin occupancy is due to varied transfection efficiency. These results suggest that TOC1 recruits NF-YC9 and HDA15 to the promoter of *AT5G02580* and *CDF5* to repress their expression, whereas the chromatin residence of HDA15 and NF-YC9 at *PIL1* also requires PRR5.

TOC1 phosphosites required for full repression of target promoter activity

We have shown that the chromatin residence of 5X is significantly reduced, and the expression of the target genes is de-repressed in 5X. To further test whether the repressive activity of 5X is altered, we transiently expressed GFP-TOC1 or GFP-5X in *toc1* protoplasts with *AT5G02580:LUC* and *CDF5:LUC* as reporters. Relative to the GFP control, we found a 77% and 58% reduced expression of *AT5G02580:LUC* by GFP-TOC1 and GFP-5X, respectively, indicating weaker repressive activity of GFP-5X (Fig 9C). To test whether HDA15 acts as a co-repressor of *AT5G02580*, we also examined the repression activity of TOC1 and 5X in *hda15 toc1*. Loss of HDA15 resulted in a decrease in repression activity of both GFP-TOC1 and GFP-5X on *AT5G02580* promoter by 1.5- and 1.4-fold, respectively (Fig 9C).

Using *CDF5:LUC* as reporter, we found GFP-TOC1 and GFP-5X exerted strongly reduced *CDF5:LUC* expression by more than 95%, and no significant difference was observed between TOC1 and 5X (Fig 9D). In the absence of HDA15, repression by TOC1 was 40% reduced, but the high variation between trials diminished statistical significance (Fig 9D) despite similar transfection efficiencies (Appendix Fig S9C). This difference between *AT5G02580* and *CDF5* may come from the very strong responsivity of *CDF5* to *TOC1* overexpression (note near tenfold difference in scale between Fig 9C and D).

PRR5 physically interacts with NF-YCs and HDA15

The strong difference in chromatin occupancy of NF-YC9 and HDA15 at *PIL1* in *prr5 toc1* compared to *toc1* suggests that PRR5 may help stabilize NF-YC9 and HDA15 residence at a subset of PHGs. Using Co-IP assays, we found weak interactions between PRR5 and NF-YC3/4/9 but none between PRR5 and NF-YB2/3, similar to the TOC1 results (Figs 10A and EV4A). Co-expression of NF-YB2 with PRR5 and NF-YC3/4/9 enhances the PRR5 and NF-YC3/C4/9 association, and NF-YB2 now appears in the immunoprecipitates (Figs 10A and EV4A), similar to the results of TOC1. This is also consistent with recent findings of PRR5, NF-YB2, and NF-YC3 (Shen *et al*, 2020). However, there was little enhancement and no Co-IP observed with NF-YB3, indicating that PRR5 may have roles divergent from TOC1. Deletion of the CCT domain from PRR5 results in weaker association between PRR5, NF-YB2, and NF-YC3/9 (Fig EV4B and C), suggesting the CCT domain is critical for the enhancement of PRR5 interaction by NF-YB2. Additionally, HDA15 was also Co-IPed with PRR5, similar to TOC1 (Fig 10B). These results show PRR5 can recruit NF-YB/C subunits and HDA15 to repress hypocotyl growth genes collaboratively with TOC1.

PRR5 and TOC1 synergistically repress hypocotyl gene expression

Previous reports indicate that PRRs are present at the same promoter regions, such as the G-box, to regulate common target genes (Liu *et al*, 2016; Zhang *et al*, 2020). *PIL1*, *AT5G02580*, and *CDF5* are common targets of PRRs (Soy *et al*, 2016; Martin *et al*, 2018; Zhang *et al*, 2020). To test the effect of PRR5 on TOC1's chromatin residence, we determined the presence of TOC1 and 5X at the promoter of *PIL1*, *AT5G02580*, and *CDF5* in *toc1* vs. *prr5 toc1* by ChIP-qPCR. For *At5G02580* and *CDF5*, there was significantly greater enrichment of TOC1 at the target promoters in *prr5 toc1* (Fig 10C), suggesting that PRR5 may compete with TOC1 for binding. In contrast, 5X enrichment appeared independent of the presence or absence of PRR5, though this may be due to the lower protein expression of 5X in *prr5 toc1* than in *toc1* at ZT14 (Fig EV4D).

To further determine whether PRR5 acts as a repressor of PHGs, we examined the expression of *PIL1*, *AT5G02580*, and *CDF5* in Col-0, *prr5*, *toc1*, and *prr5 toc1* at ZT18. The absence of PRR5 did not alter target gene expression, whereas deletion of both TOC1 and PRR5 leads to synergistically greater expression of *PIL1*, *AT5G02580*, and *CDF5* (Fig 10D). The *prr5 toc1* period is only 0.7 h shorter than *toc1* under constant white light (Appendix Fig S10B). Given that our gene expression and ChIP assays were done under entraining conditions (8:16; light:dark cycles), it is likely that the phasing difference between these two backgrounds is relatively small and not likely to account for the differences in gene expression in Fig 10D.

Hypocotyl growth under constant red light with sequential fluence rates showed only modest lengthening (at one fluence rate tested) in *prr5* relative to Col-0 (Appendix Fig S10A). In contrast, *prr5 toc1* displayed synergistically enhanced hypocotyl elongation compared with *prr5* or *toc1* single mutants (Appendix Fig S10A), consistent with previous findings (Ito *et al*, 2008) and our gene

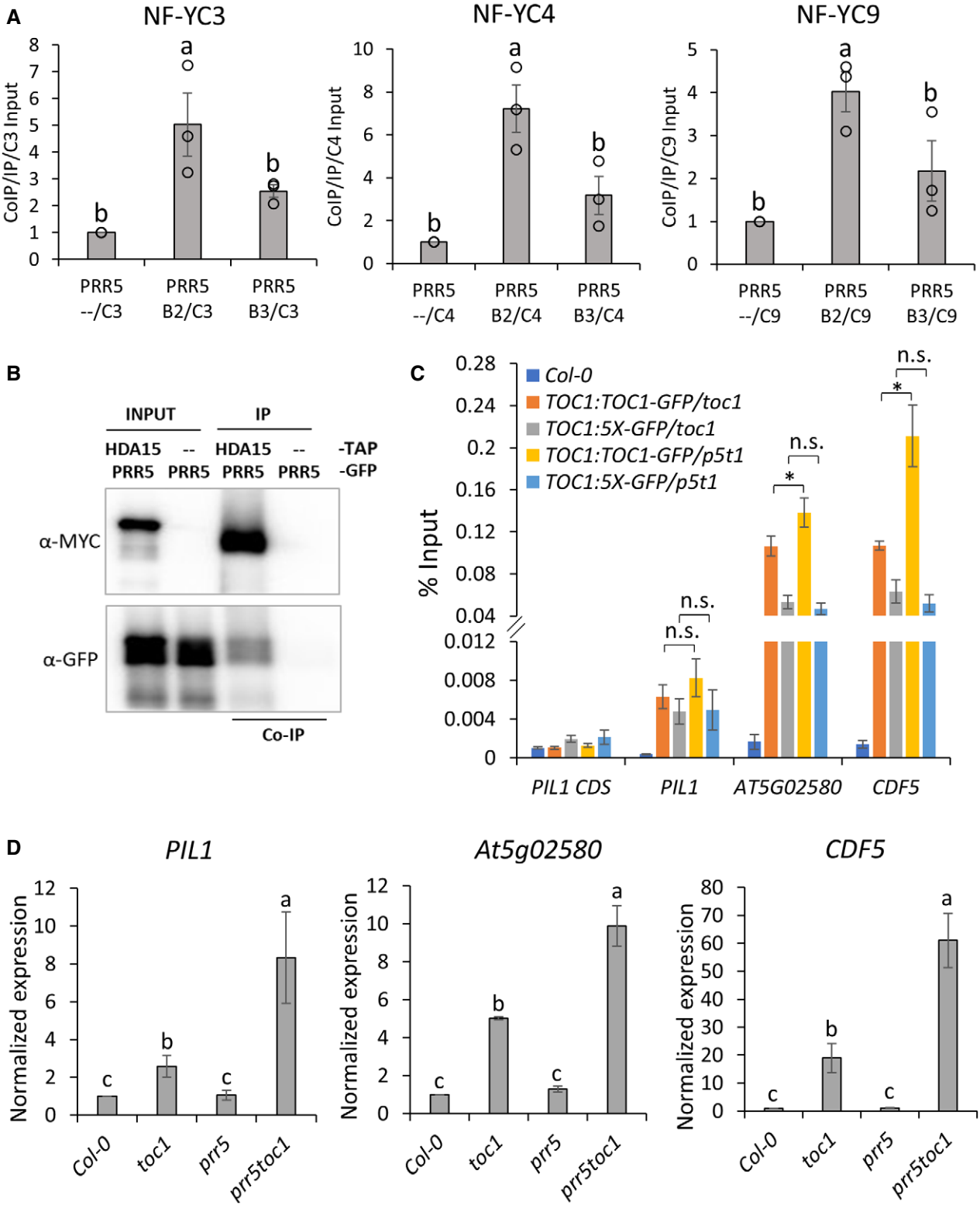

Figure 10.

Figure 10. NF–YB/C subunits and HDA15 physically interact with PRR5.

A Quantification of interactions between TAP-PRR5 and NF-YC proteins in the presence or absence of NF-YB subunits. Proteins were transiently expressed in *N. benthamiana*. TAP-PRR5 was immunoprecipitated with IgG resins followed by HRV-3C protease digestion. PRR5 and NF-YB/C were detected by α-MYC and α-HA, respectively. Protein band intensity was measured by ImageJ, and interactions were exhibited as ratio of co-immunoprecipitated NF-YC to immunoprecipitated PRR5 to NF-YC input. Results from 3 independent trials were averaged. Error bars indicate SEM, and different letters denote significant differences ($P < 0.05$, Student's *t*-test).

B Co-IP of HDA15-TAP and GFP-PRR5 in *N. benthamiana*. HDA15-TAP was immunoprecipitated with IgG resins and digested by HRV-3C protease. HDA15 and PRR5 were detected by α-MYC and α-GFP, respectively. Results represent two independent trials.

C ChIP-qPCR of TOC1-GFP and 5X-GFP binding to the target promoters at ZT14 in *toc1* vs. *prr5 toc1* (*p5t1*) mutant. 3-d-old SD-grown seedlings were harvested at ZT14, TOC1 and 5X were immunoprecipitated by α-GFP. Data from 3 independent trials were averaged, and error bars indicate SEM. Asterisks indicate significant differences (Student's *t*-test; $*P < 0.05$), n.s. = not significant.

D Expression of *PIL1*, *AT5G02580*, and *CDF5* in 3-d-old SD-grown seedlings at ZT18. Data from 3 biological trials were averaged. Error bars indicate SEM. Different letters denote statistically significant differences based on Wilcoxon test ($P < 0.05$).

Source data are available online for this figure.

expression results (Fig 10D). Taken together, these results suggest that PRR5 and TOC1 act together to repress hypocotyl growth through a similar mechanism.

Discussion

An NF-YB/NF-YC/TOC1 repressor complex, NF-TOC1

To better understand the role of phosphorylation in the function of TOC1, the founding member of the PRR family, we have identified key phosphorylation sites which establish the importance of N-terminal phosphosites for TOC1 stability, chromatin residence, and interaction with members of the NF-Y transcription factors.

NF-Y transcription factors are important transcriptional regulators of developmental and stress responses (reviewed in ref. Myers & Holt, 2018) and are composed of 3 subunits, NF-YA, NF-YB, and NF-YC, each of which is multi-member gene families conserved among plant genomes (Petroni *et al*, 2012). NF-YB and NF-YC first form a histone fold domain (HFD) which then recruits the DNA-binding subunit, NF-YA which contains a CONSTANS, CONSTANS-like, and TOC1 (CCT) C-terminal domain to control downstream gene expression as a trimeric transcriptional complex (Petroni *et al*, 2012; Hou *et al*, 2014; Zhao *et al*, 2016). NF-YA can be replaced by CCT domain-containing proteins, such as CONSTANS (CO), to regulate flowering (Wenkel *et al*, 2006). Additionally, gel electrophoresis mobility shift assays (EMSAs) have shown CCT domain proteins such as CO require NF-YB and NF-YC partners for DNA binding (Gnesutta *et al*, 2017; Chaves-Sanjuan *et al*, 2021; Lv *et al*, 2021) and for PRR protein binding to the *LHY* promoter (Shen *et al*, 2020). Our results, together with these *in vitro* reports, support TOC1 as an *in vivo* NF-YA-like partner in association with NF-YB/C subunits (Figs 7 and 9B, Appendix Fig S6), and we term this NF-YB/NF-YC/TOC1 repressor complex NF-TOC1.

A connection between photomorphogenesis and NF-Y factors has been previously established. *NF-YC* genes redundantly repress hypocotyl elongation in constant light and under short days (Myers *et al*, 2016; Tang *et al*, 2017). NF-YC9 associates with ELONGATED HYPOCOTYL 5 (HY5) to co-regulate a subset of photomorphogenic-related genes (Myers *et al*, 2016) and also interacts with HDA15 to repress a group of hypocotyl growth-related genes (Tang *et al*, 2017). However, genetic evidence showed NF-YC function is at least partially independent of HY5 and HDA15 (Myers *et al*, 2016; Tang *et al*, 2017), suggesting that other partners are involved in NF-Y-mediated photomorphogenesis. Our work clearly connects the role of TOC1 in photomorphogenesis to these same components.

In support of previous work (Soy *et al*, 2016), we find that TOC1 chromatin residence at key PHGs does not require the presence of PIF3, PIF4, or PIF5 (Fig 5D). While it is possible that other PIFs help anchor TOC1 to the promoter (Zhang *et al*, 2020), we consider this unlikely as TOC1 residence was strongly diminished in the NF-YC triple mutant (Fig 7C), supporting the notion that NF-Y B and C subunits stabilize TOC1 chromatin binding, as reported for other NF-Y heterotrimers (Gnesutta *et al*, 2017). The continued chromatin presence of TOC1 at target promoters in the *nf-yc3/4/9* triple mutant may result from NF-YC redundancy as *nf-yc1/3/4/9* quadruple mutants have longer hypocotyls than the triple mutant (Tang *et al*, 2017). Reciprocally, NF-YC9 chromatin residence at PHGs was reduced to near background levels in *toc1-101*, indicating TOC1 is fully required to anchor NF-YC (Fig 9B).

A TOC1 and PRR5 relationship

Similarities between *toc1* and *prr5* phenotypes have suggested possible similar molecular mechanisms (Martin *et al*, 2018; Zhang *et al*, 2020). We find that PRR5 also likely forms a NF-YB/NF-YC/PRR5 trimeric transcriptional repressor, with only slight differences from TOC1 in the effectiveness of specific NF-YBs in facilitating interactions between NF-YC and TOC1 or PRR5 (compare Figs 7B and 10A). With ~10 members each of the NF-YB and NF-YC families in *Arabidopsis* (Petroni *et al*, 2012), there is great potential for subtle and specific differences in the pairings with TOC1 and PRR5 to allow a high degree of nuance in TOC1 and PRR5 downstream effects.

At the same time, PRR5 can act additively with TOC1 in facilitating NF-YC and HDA15 chromatin residence at some gene promoters (e.g., PIL1) (Fig 9A and B). This further supports an NF-YB and NF-YC model for PRR5 action and indicates that HDA15 can be part of the PRR5 repressor complex. As PRR5 directly interacts with the co-repressor TOPLESS (TPL) (Wang *et al*, 2013), this finding is consistent with a PRR5-TPL-HDA15 complex at these promoters, as previously described for PRR9 and HDA6 (Wang *et al*, 2013). However, PRR5 can directly Co-IP with HDA15 (Fig 10B), suggesting that TPL is not strictly required but may enhance HDA association with PRR5. In contrast, TOC1 cannot interact with TPL (Wang *et al*, 2013) but associates directly with HDA15, in a phosphorylation-

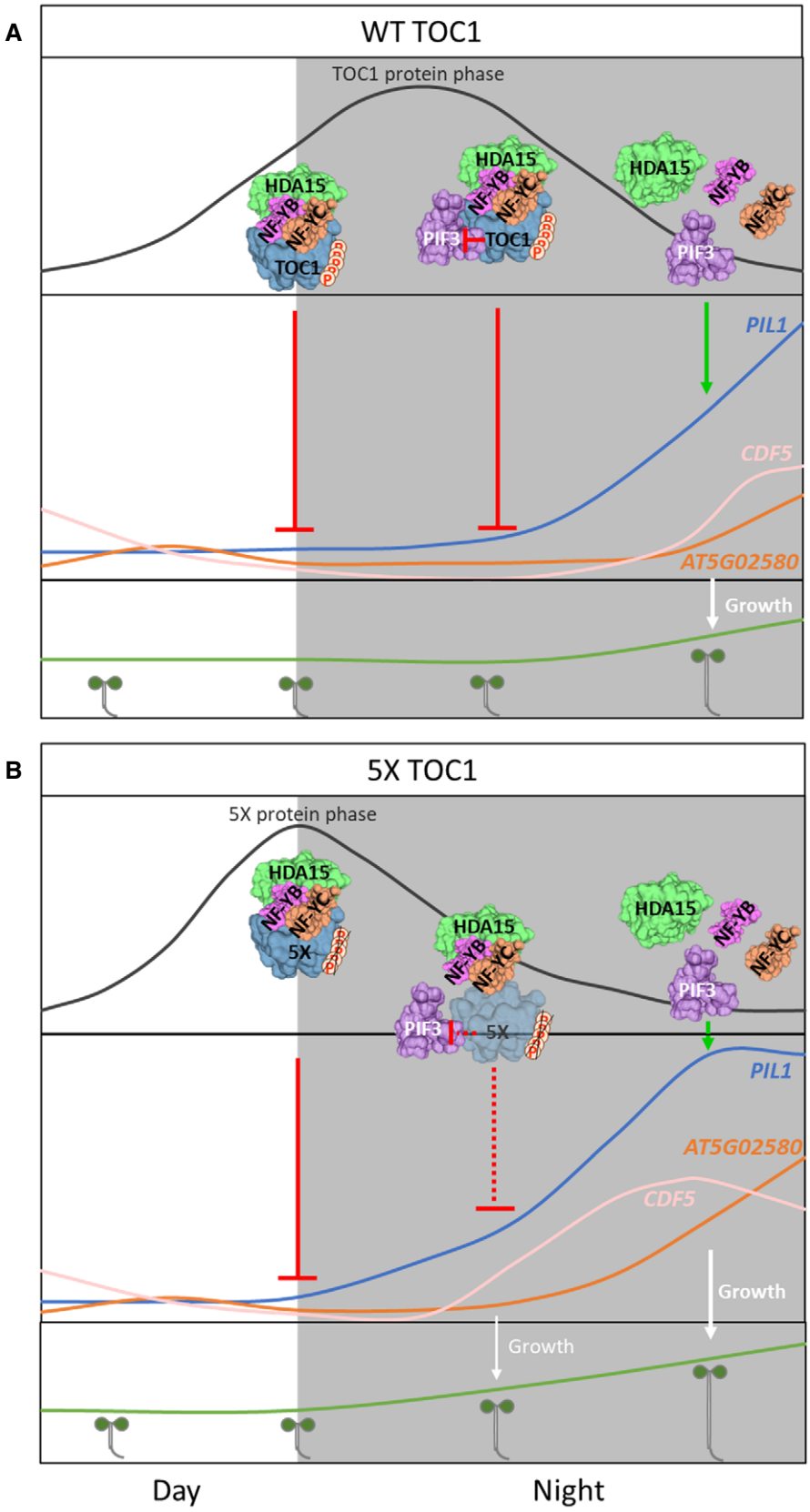

Figure 11.

Figure 11. Proposed mechanism for the role of TOC1 phosphorylation in the control of hypocotyl growth.

A, B At early night, wild-type (A) and 5X (B) TOC1 are equally present and recruit transcriptional repressors NF-YB/C and HDA15 with PRR5 (not shown) to inhibit expression of PHGs. As night progresses, PIF3 levels rise, and the advanced phase of 5X, more rapid degradation and poorer PIF3 interaction result in lesser presence of 5X at target promoters, relative to wild-type TOC1, leading to attenuated inhibition of PHGs and enhanced hypocotyl growth. At late night, low TOC1 and PRR5 levels reduce NF-YB/C and HDA15 recruitment, resulting in PIF3 release to activate downstream PHGs that leads to maximal pre-dawn hypocotyl growth.

enhanced way (Fig 8A and B). This highlights a fundamental difference between TOC1 and PRR5 repressor complex composition, although histone deacetylation is common to both.

In some cases, PRR5 appears to interfere with TOC1 binding (e.g., *CDF5* and *At5g02580*), with TOC1 chromatin residence increased in the absence of PRR5 (Fig 10C). PRR5 and TOC1 both bind G-box sequences (Huang *et al*, 2012; Liu *et al*, 2016), and the two G-box instances in the *CDF5* and *At5g02580* promoters are only separated by 62 and 96 nucleotides, respectively (Soy *et al*, 2016; Martin *et al*, 2018). This close positioning supports the notion of binding site competition among the PRRs (Liu *et al*, 2016). This observation also suggests that direct TOC1-PRR5 oligomerization, which facilitates TOC1 nuclear accumulation and phosphorylation (Wang *et al*, 2010), does not enhance TOC1 chromatin binding.

In the context of the genes examined here, PRR5 is the less effective factor at ZT18. The absence of PRR5 alone has no effect on *PIL1*, *At5g02580*, and *CDF5* expression, compared with the *toc1* mutant, and TOC1 appears to effectively replace PRR5 when it is absent. However, PRR5 is not equally effective in compensating TOC1 absence, and with both gone de-repression is strongly enhanced (Fig 10D). The relative levels of TOC1 and PRR5 are likely important in this difference in effectiveness, with PRR5 levels waning while TOC1 remains high late in the night (Fujiwara *et al*, 2008). Additionally, indirect effects of PRR5 absence earlier in the day may affect the presence of unknown factors necessary to later work with TOC1 in effecting transcriptional repression.

Complexity of TOC1 phosphorylation

Recent work suggests one or more members of the casein kinase 1-like family (CKL) can phosphorylate TOC1. CKL4 phosphorylates PRR5 and TOC1 *in vitro*, and inhibition of CKL activity by PHA767491 increases levels of TOC1 and PRR5 *in vivo* (Uehara *et al*, 2019). This inhibitor lengthens circadian period, consistent with an increase in TOC1 and PRR5 proteins. It is unlikely this kinase family is responsible for phosphorylating the sites described here, as the phospho-mutations we identified cause shorter period and reduced stability of TOC1. Additionally, we detect a marked mobility shift in WT TOC1-GFP, which is largely eliminated in 5X and S175A (Fig 1C). Such a change in mobility was not observed for TOC1 in the kinase-deficient Uehara *et al* work, though differences in gel conditions might account for this.

These results suggest at least one other different kinase or kinase class is involved in the phosphorylation near the N-terminus of TOC1. Two kinase prediction programs (Scansite 4.0, https://scansite4.mit.edu/#home; NetPhos3.1, http://www.cbs.dtu.dk/services/NetPhos/) return CK II as the most likely kinase responsible for S175 phosphorylation, and future work will be testing this and other possibilities.

Other findings (Fujiwara *et al*, 2008) have implicated a phosphorylation-dependent interaction between TOC1 and ZTL, which when absent would diminish TOC1 protein turnover, leading to a longer period. Hence, other sites, possibly more C-terminal to the sites described here, and phosphorylated by CKL family members, may be involved in facilitating the phosphorylation-enhanced TOC1-ZTL interaction.

The five phosphorylation sites are not equally important in determining TOC1 functionality. The *S175A* mutation was most similar to the *5X* mutant in the effect on gel migration of the PRR5-mediated phosphorylation of the N-terminal domain, whereas mutations at the other four sites showed migration profiles closer to WT (Fig 1B). The effect of phosphatase treatment on full-length S175A and 5X protein gel migration was also similarly minimal (Fig 1C). Both mutant forms showed similar effects on hypocotyl length (Figs 2 and 3A; Appendix Fig S2), period (Fig 3B), flowering time (Appendix Fig S3C), TOC1 stability (Fig 6B and C), *CDF5* expression (Fig EV1), and phasing of TOC1 expression (Figs 6A and EV2A). In some cases, the *5X* mutant more poorly complements *toc1-101* than does *S175A* (see Fig EV1; *PIL1* and *At5g02580* gene expression and Fig 2B and D; hypocotyl length in red light). This suggests that one or more of the other phosphosites contributes to TOC1 function in addition to S175. The close proximity of three sites (S194, S201, and T204) suggests phosphorylation by the same kinase (Schweiger & Linial, 2010), and future work will determine whether this cluster works together with S175 in effecting the full activity of phosphorylated TOC1.

Interestingly, while none of the five identified TOC1 phosphosites is conserved among the other four *Arabidopsis* PRR proteins (Fig EV5A), S175 is the only one of the 5 residues perfectly conserved among other TOC1-like proteins found in a wide range of plant and algal species (Fig EV5B) including the microalgae *Ostreococcus tauri* (Fig EV5C). These findings provide further evidence of the importance of this residue for TOC1 function.

Intersection of circadian regulation and photomorphogenesis

The short period of *toc1* shifts the maximal expression of clock regulated genes and proteins to earlier in the day even under light–dark cycles (Fig 4). The unique properties of the *5X* mutant allow nearly normal levels of TOC1 accumulation to occur at an earlier phase, partially separating the short period normally associated with a *toc1* null from the complete absence of the protein. While TOC1 5X is compromised in function, it is clear that its phase advance (Figs 6A and EV2A) shifts its maximal repressive activity to earlier in the night, allowing an earlier de-repression of key PHG's, resulting in increased hypocotyl elongation (Fig 11A and B). The diminished chromatin residence of 5X, arising from reduced NF-YC interaction, combined with reduced 5X activity, resulting from lesser HDA15 and PIF3 interactions, highlights the multifunctional role of these N-terminal phosphorylations (Fig 11A and B). These findings are currently limited to the role of TOC1 in light mediated hypocotyl growth, but recent *in vitro* findings substantiating NF-TOC1 trimers

at the *LHY* promoter (Shen *et al*, 2020) suggest similar complexes will form the core of the repressive activity of most PRR proteins.

Materials and Methods

Plant materials and growth conditions

The wild-type and all mutants of *Arabidopsis thaliana* used in this study were of the Colombia-0 (Col-0) ecotype. The *toc1-101* (*toc1* (Kikis *et al*, 2005)), *pif3-3 pif4-2 pif5-3* (*pif3/4/5* (Soy *et al*, 2016)), *hda15-1* (*hda15* (Liu *et al*, 2013; Tang *et al*, 2017)), *prr5-1* (*prr5* (Eriksson *et al*, 2003)), and *nf-yc3-1 nf-yc4-1 nf-yc9-1* (*nf-yc3/4/9* (Kumimoto *et al*, 2010)) mutant lines, and the *CCA1:LUC* line (Salome & McClung, 2005) were previously described. The *hda15-1* (SALK_004027) and *prr5-1* (SALK_006280) were obtained from the *Arabidopsis* Biological Resource Center (http://www.arabidopsis.org/), and the *pif3-3 pif4-2 pif5-3* and *nf-yc3-1 nf-yc4-1 nf-yc9-1* are kind gifts from Dr. Elena Monte and Dr. Ben Holt III, respectively. The *toc1-101* was crossed with *hda15-1*, *prr5-1*, and *nf-yc3/4/9* to produce *hda15 toc1*, *prr5 toc1*, and *nf-yc3/4/9 toc1*, respectively. To generate transgenic lines harboring *TOC1:TOC1*, the 35S promoter of vector pMDC85 was replaced by the *TOC1* native promoter (−2354 to +1 of ATG). The coding sequence of *TOC1* was placed in frame with the GFP tag in pMDC85 by LR recombination. To generate transgenic lines harboring *35S:TOC1*, the coding sequence of *TOC1* was cloned upstream of GFP tag into vector pMDC85. The point mutations in *5X*, *135A*, and *175A* were introduced by site-directed mutagenesis and inserted into pMDC85 with the *TOC1* native promoter or 35S promoter to create the destination expression clone. Independent T1 transgenic plants were obtained through *Agrobacterium*-mediated transformation into *toc1-101* carrying *CCA1:LUC*. Lines with a 3:1 segregation ratio on hygromycin plates were homozygosed for further studies. To generate *TOC1* native promoter lines in *hda15 toc1*, *prr5 toc1*, *pif3/4/5 toc1*, and *nf-yc3/4/9 toc1* backgrounds, the selected homozygous *TOC1:TOC1/toc1* or *TOC1:5X/toc1* was crossed into *hda15*, *prr5*, *pif3/4/5*, and *nf-yc3/4/9*, respectively. Homozygous F3 progenies of each plant line were used for ChIP assays.

Seeds were surface sterilized and stratified at 4°C for 4 days, and seedlings were all grown at 22°C. For bioluminescence acquirement and period estimates, seedlings were entrained under 12-h white fluorescent light (50 μmol m^{-2} s^{-1})/12-h dark cycles for 7 days on MS (Murashige and Skoog) plates with 3% sucrose and 0.8% agar as previously described (Somers *et al*, 2004). Seedlings were then subject to constant red (30 μmol m^{-2} s^{-1}) or white (50 μmol m^{-2} s−1) light as indicated in a Percival E30LEDL3 growth chamber (Percival Scientific, Perry, IA). Seedlings for hypocotyl measurements at various fluence rates of constant red light were grown on MS without sucrose as previously described (Fankhauser & Casal, 2004). For hypocotyl measurements, protein immunoblotting, transcript abundance analyses, and ChIP assays in short day (SD) conditions, seedlings were grown under 8-h white fluorescent light (50 μmol m^{-2} s^{-1})/16-h dark cycles for 3 days on MS plates with 0.8% agar without sucrose. For phosphatase assays, cycloheximide (CHX) treatments, and nucleocytoplasmic fractionation, seedlings were grown under 12-h white fluorescent light (50 μmol m^{-2} s^{-1})/12-h dark cycles for 10 days on MS plates with 3% sucrose and 0.8% agar. For transient expression experiments, 4-week-old *N. benthamiana* were infiltrated with *Agrobacteria* as described earlier (Fujiwara *et al*, 2008). Tissues were harvested on the third day at ZT12 (16-h light/8-h dark).

Constructs

To construct TAP-tagged TOC1 CCT domain (533–574 aa), TOC1ΔCCT (1–527 aa), PRR5 full-length, PRR5ΔCCT (1–508 aa), and HDA15 full-length expression clones, primers listed in Appendix Table S1 were used to amplify corresponding fragments. Each amplicon was subcloned into pENTR/D-TOPO and placed upstream of the TAP tag by LR recombination (Invitrogen) into the binary vector pYL436 (ABRC; CD3–679). Full-length, N-terminus (1–242 aa) *TAP-TOC1*, *TAP-PRR5*, and *PRR5-GFP* constructs were assembled as described earlier (Wang *et al*, 2010). TOC1 point mutations were generated in pENTR2B-TOC1 using primers listed in Appendix Table S1. *PIF3-TAP* (DKLAT1G09530) was obtained from ABRC. To generate *TOC1-GFP*, *5X-GFP*, *PIF3-YFP-HA*, *NF-YB-HA*, and *NF-YC-HA* expression clones for co-IP assays in *N. benthamiana*, the cDNA fragments of each gene were subcloned into pENTR2B or pENTR/D-TOPO and placed into the binary vector pMDC85, pEarleyGate101, or pCsVMV-HA_3-N-1300 by LR recombination.

To generate plasmids for transient expression in protoplasts, the cDNA fragments of *TOC1*, *5X*, *HDA15*, and *NF-YC9* were transferred from pENTR/D-TOPO entry clones to pCsVMV:GFP-C-999 destination vector by LR recombination. To generate reporter plasmids for transient repression assay, the promoter region of *AT5G02580* (−1936 to +1 of ATG) and *CDF5* (−2122 to +1 of ATG) was amplified and subsequently digested by BamHI/HindIII and SacII/HindIII, respectively. The fragments were then placed upstream of firefly luciferase reporter by replacing *CCA1* promoter in *CCA1pro:FLuc* that was previously used in Wang *et al* (2013).

To construct plasmids for Y2H assay tests between TOC1 and NF-YB/C, Gateway entry clones of full-length *TOC1* and *5X* were recombined into the ProQuest Two-Hybrid System (Invitrogen) vector pDEST22 carrying Gal4 activation domain. *NF-YB/C* was cloned into pDEST32 vector carrying Gal4 DNA-binding domain as previously described (Kumimoto *et al*, 2010). For Y2H assay of dimerization between TOC1 and 5X, full-length *TOC1* and *5X* were placed in pGBKT7 or pGADT7 vector of the Matchmaker Gold Two-Hybrid System (Takara).

Mass spectrometry analysis

The following protocols were followed for the identification of the S175, S194, S201, and T204 phosphosites. In-gel digestions were performed as described previously (Shevchenko *et al*, 2006). Digested peptides in the gel pieces were recovered by adding 5% formic acid/acetonitrile, desalted using StageTips with C18 disk membranes (EMPORE, 3 M) (Rappsilber *et al*, 2003), dried in a vacuum evaporator, and dissolved in 9 μl of 5% acetonitrile containing 0.1% trifluoroacetic acid. An LTQ-Orbitrap XL (Thermo Fisher Scientific) coupled with an EASY-nLC 1000 (Thermo Fisher Scientific) was used for nano-LC-MS/MS analyses. A self-pulled needle (150 mm length × 100-μm i.d., 6-μm opening) packed with ReproSil C18 resin (3 μm; Dr. Maisch GmbH) was used as an analytical column with "stone-arch" frit (Ishihama *et al*, 2002). A spray

voltage of 2,400 V was applied. The injection volume was 6 µl, and the flow rate was 500 nl min^{-1}. The mobile phase consisted of 0.5% acetic acid (A) and 0.5% acetic acid and 80% acetonitrile (B). A two-step linear gradient of 0% to 40% B in 30 or 60 min, 40% to 100% B in 5 min, and 100% B for 10 min was employed. The MS scan range was m/z 300–1,400. The top 10 precursor ions were selected in the MS scan by Orbitrap at 100,000 resolution and for subsequent MS/MS scans by ion trap in the automated gain control mode, where automated gain control values of 5.00e + 05 and 1.00e + 04 were set for full MS and MS/MS, respectively. The normalized collision-induced dissociation was set to 35.0. A lock mass function was used for the LTQ-Orbitrap XL to obtain constant mass accuracy during gradient analysis (Olsen *et al*, 2005). Multistage activation was enabled upon detection of a neutral loss of phosphoric acid (98.00, 49.00, or 32.66 a.m.u.) (Schroeder *et al*, 2004) for further ion fragmentation. Selected sequenced ions were dynamically excluded for 60 s after sequencing. Mass Navigator version 1.3 (Mitsui Knowledge Industry, Tokyo, Japan) with default parameters for LTQ-Orbitrap XL was used to create peak lists on the basis of the recorded fragmentation spectra. The m/z values of the isotope peaks were converted to the corresponding monoisotopic peaks when the isotope peaks were selected as the precursor ions. To improve the quality of the MS/MS spectra, Mass Navigator discarded all peaks of < 10 absolute intensity and with < 0.1% of the most intense peak in MS/MS spectra (Ravichandran *et al*, 2009). Peptides and proteins were identified by means of automated database searching using Mascot version 2.3.02 (Matrix Science) in The *Arabidopsis* Information Resource database (TAIR10_pep_20101214,https://www.arabidopsis.org/download/index-auto.jsp?dir = %2Fdownload_files%2FProteins%2FTAIR10_protein_lists) containing protein sequence information of the Myc-tagged N-terminal portion of TOC1s with a precursor mass tolerance of 3 ppm, a fragment ion mass tolerance of 0.8 Da, and strict trypsin specificity (Olsen *et al*, 2004), allowing for up to two missed cleavages. Carbamidomethylation of Cys was set as a fixed modification, and oxidation of Met and phosphorylation of Ser, Thr, and Tyr were allowed as variable modifications. The data have been deposited in jPOST under the accession number JPST001185 (Okuda *et al*, 2017).

The T135 phosphosite was separately identified using the following protocols. After gel staining, sample lanes were separated into 8 fractions. Each fraction was divided into small cubes and transferred to a 96-well plate (1 fraction/well). Digestion and extraction were performed by the Ettan Spot Handling Workstation 2.1 (User Manual from Amersham Biosciences). Gel pieces were washed in 100 µl of 50% methanol/5% acetic acid for 30 min. The gel pieces were next washed with acetonitrile for 10 min. then dried, and suspended in 75 ml 50 mM ammonium bicarbonate (with 5 mg/ml DTT) for 30 min at room temperature (RT). The DTT-containing ammonium bicarbonate was aspirated, and the gel pieces were suspended in 50 mM ammonium bicarbonate containing 15 mg/ml iodoacetamide and incubated for 30 min. in the dark at RT. The gel pieces were then alternately incubated with 50 mM ammonium bicarbonate and acetonitrile, respectively, for 10 min. each (total of four incubations) and then completely dried. Dried gel slices were rehydrated with 25 ml of 50 mM ammonium bicarbonate. 75 µl of sequencing grade-modified trypsin (Promega, Madison WI) prepared at 10 µg/ml in 50 mM ammonium bicarbonate was added and then driven into the gel pieces for 15 min at 37°C. Finally, 25 ml 50 mM ammonium bicarbonate was added to the trypsin mix and digestion took place for overnight. The peptides were extracted from the polyacrylamide with 50 µl 50% acetonitrile and 5% formic acid three times. A final extraction with 50 ml of acetonitrile was performed. The extracted pool was completely dried in a vacufuge and peptides were resuspended in 20 ml of 50 mM acetic acid.

Capillary-liquid chromatography tandem mass spectrometry (Cap-LC/MS/MS) was performed on a Thermo Scientific LTQ mass spectrometer equipped with a CaptiveSpray source (Bruker Daltonics Billerica, MA) operated in positive ion mode. The LC system was an UltiMate™ 3000 system (Thermo Scientific). Solvent A was water containing 50 mM acetic acid, and solvent B was acetonitrile. 5 ml of each sample was first injected onto the m-Precolumn Cartridge (Thermo Scientific) and washed with 50 mM acetic acid. The injector port was switched to inject, and the peptides were eluted off of the trap onto the column. A 0.2 × 150 mm, 3u, 200A, Magic C18 (Bruker Daltonics Billerica, MA) was used for chromatographic separations. Peptides were eluted directly off the column into the LTQ system using a gradient of 2–80%B over 45 min, with a flow rate of 2 µl/min, and total run time of 60 min. The MS/MS was acquired according to standard conditions established in the lab. Briefly, a CaptiveSpray source operated with a spray voltage of 3 KV and a capillary temperature of 200PoPC is used. The scan sequence of the mass spectrometer was based on the TopTen™ method; the analysis was programmed for a full scan recorded between 350 and 2,000 Da, and a MS/MS scan to generate product ion spectra to determine amino acid sequence in consecutive instrument scans of the ten most abundant peak in the spectrum. The AGC Target ion number was set at 30,000 ions for full scan and 10,000 ions for MSn mode. Maximum ion injection time was set at 20 ms for full scan and 300 ms for MSn mode. Micro scan number was set at 1 for both full scan and MSn scan. The CID fragmentation energy was set to 35%. Dynamic exclusion was enabled with a repeat count of 2 within 10 s, a mass list size of 200, an exclusion duration 350 s, the low mass width was 0.5, and the high mass width was 1.5.

Sequence information from the MS/MS data was processed by converting the.raw files into a merged file (.mgf) using an in-house program, RAW2MZXML_n_MGF_batch (merge.pl, a Perl script). The resulting mgf files were searched using Mascot Daemon by Matrix Science version 2.3.2 (Boston, MA) and the database searched against the most recent SwissProt or NCBI databases. The mass accuracy of the precursor ions was set to 1.8 Da, and the fragment mass accuracy was set to 0.8 Da. Considered variable modifications were methionine oxidation, deamidation NQ, and phosphorylation. Fixed modification for carbamidomethyl cysteine was considered. Two missed cleavages for the enzyme were permitted. A decoy database was searched to determine the false discovery rate (FDR), and peptides were filtered according to the to the FDR and proteins identified required bold red peptides. Protein identifications were checked manually, and proteins with a Mascot score of 50 or higher with a minimum of two unique peptides from one protein having a -b or -y ion sequence tag of five residues or better were accepted. Identified phosphorylated peptides were verified manually.

Protein extraction and immunoblots

Total protein extraction was carried out as described earlier (Kim *et al*, 2007; Fujiwara *et al*, 2008). For the immunoblot analyses, proteins were separated by 10% SDS–PAGE (acrylamide:bisacrylamide 37.5:1), 8% SDS–PAGE (acrylamide:bisacrylamide 150:1, to differentiate wild-type and phosphosite mutants of TOC1), or 12% SDS–PAGE (acrylamide:bisacrylamide, 37.5:1) for histone H3 and GFP alone. Immunoblotting was performed using 1:5,000 dilution of primary polyclonal anti-GFP (Abcam ab6556), 1:2,000 dilution of primary anti-histone H3 (Abcam 1791), 1:10,000 dilution of polyclonal ADK primary antibodies (gift from Dr David Bisaro) (Mohannath *et al*, 2014), 1:200 dilution of primary anti-GAL4DBD (Santa Cruz sc-577) followed by ECL detection using anti-rabbit IgG with horseradish peroxidase (HRP) linked whole antibody (GE Healthcare NA934V). For immunoblotting of primary anti-Myc (Sigma-Aldrich M4439, 1:4,000 dilution), HRP-linked anti-mouse IgG (Sigma-Aldrich A0198, 1:1,000 dilution) was used as secondary antibody. Chemiluminescence reactions were performed with Supersignal West Pico and Femto Chemiluminescent Substrates (Thermo Scientific).

Yeast two-hybrid assay

The bait and prey clones were constructed into the ProQuest Two-Hybrid System (Invitrogen) vectors pDEST22 and pDEST32 as described above, and sets of constructs were co-transformed into yeast strain AH109 (*MATa*, *trp1-901*, *leu2-3*, *112*, *ura3-52*, *his3-200*, *gal4Δ*, *gal80Δ*, *LYS2::GAL1*$_{UAS}$-*GAL1*$_{TATA}$-HIS3, *GAL2*$_{UAS}$-*GAL2*$_{TATA}$-ADE2, *URA3::MEL1*$_{UAS}$-*MEL1*$_{TATA}$-lacZ). Yeast transformants were selected on glucose-based synthetic minimal medium (SD; 0.67% yeast nitrogen base, 2% glucose (wt/vol), and amino acid dropout solution) deficient in leucine and tryptophan (-L-W), and protein interaction tests were performed on SD-LEU-TRP-HIS media with 5 mM 3-AT. To test the dimerization of TOC1/5X, the bait and prey clones were constructed into the Matchmaker Gold Two-Hybrid System (Takara) and co-transformed into yeast strain Y2HGold. The two-hybrid and quantitative β-Galactosidase assays were performed as instructed by manufacturer's manual (Takara, Yeast protocols handbook).

Co-immunoprecipitation (Co-IP) assays

Agrobacteria containing corresponding expression clones were coinfiltrated into 4-week-old *N. benthamiana* leaves. The infiltrated leaves were ground to fine powder in liquid nitrogen, and the proteins were extracted with ice-cold IP buffer (50 mM Tris-Cl, pH 7.5/150 mM NaCl/0.5% NP-40/1 mM EDTA/3 mM DTT/1 mM PMSF/2 mM NaF/2 mM Na_3VO_4/1 μg ml^{-1} leupeptin/1 μg ml^{-1} aprotinin/1 μg ml^{-1} pepstatin/5 μg ml^{-1} antipain/5 μg ml^{-1} chymostatin/50 μM MG132/50 μM MG115/50 μM ALLN). The cleared supernatant was used for immunoprecipitation with Human IgG-Agarose (Sigma-Aldrich, A6284). The immune complex was washed 4–5 times by IP buffer and subsequently released from resin by HRV-3C protease digestion. The eluted TAP-, GFP-, and HA-tagged proteins were detected by Western blotting using primary Myc antibody (Sigma-Aldrich, M4439), GFP antibody (Abcam, ab6556), HA antibody (Roche, 3F10), and secondary HRP-linked anti-mouse IgG (Sigma-Aldrich, A0198), HRP-linked anti-Rabbit IgG (GE Healthcare, NA934V), and HRP-linked anti-Rat IgG (Sigma-Aldrich, A5795), respectively.

Chromatin immunoprecipitation (ChIP) assays

Chromatin immunoprecipitation assays were conducted as previously described (Yamaguchi *et al*, 2014). Briefly, 3-day-old *Arabidopsis* seedlings grown in SD condition were harvested at ZT14 and cross-linked with 1% formaldehyde by vacuum infiltration. Cross-link was then quenched by 0.125 M glycine. ChIP extracts were incubated with anti-GFP (Abcam ab6556) overnight and immunoprecipitated by Protein G Dynabeads (Thermo scientific 10004D). DNA of input and reverse cross-linked IP samples was purified using QIAquick PCR clean up Kit (Qiagen) and subject to quantitative PCR using promoter-specific primers listed in Appendix Table S1.

Dual bioluminescence assay

Protoplast isolation and DNA transfection were performed as previously described (Yoo *et al*, 2007; Zhai *et al*, 2009). Each effector (GFP-TOC1 and GFP-5X) was co-transfected with *35S:Rluc* (*Renilla reniformis luciferase*) and *Fluc* (*Firefly luciferase*) reporter driven by promoter of interest (*pAT5G02580* and *pCDF5*). The bioluminescence acquirement and analysis were done as previously described (Wang *et al*, 2013).

Phosphatase assay

10-day-old seedlings of *TOC1:TOC1-GFP*, *TOC1:5X-GFP*, *TOC1:135A-GFP*, and *TOC1:175A-GFP* transgenic lines were harvested at ZT13, and the phosphatase and inhibitor treatments were performed as described (Fujiwara *et al*, 2008).

Luminescence measurement and circadian rhythm analysis

Luminescence acquirement was conducted as previously described (Somers *et al*, 2004). Data analysis and period estimate (based on *CCA1:LUC* reporter) were performed as in Wang *et al* (2013).

RNA extraction and quantitative PCR

3-day-old seedlings grown in SD conditions were harvested at indicated time points. Total RNA extraction, DNase treatment, cDNA synthesis, and quantitative PCR were done as described earlier (Wang *et al*, 2013).

Cycloheximide treatments

Plants grown under LD cycles for 10 days were transferred to continuous darkness at ZT12 and immersed into liquid MS media with 0.01% Triton X-100 and 100 μM cycloheximide (CHX) or equal amount of ethanol (Mock). Plants in the liquid media were shaken slowly for the indicated durations before harvesting. Protein extraction and immunoblotting were performed as described above.

Fractionation of cytosolic and nuclear proteins

10-day-old seedlings of *TOC1:TOC1-GFP* and *TOC1:5X-GFP* transgenic lines grown under LD cycles were harvested at indicated time points, and nucleocytoplasmic protein fractionation was carried out as described earlier (Wang *et al*, 2010).

Statistical analysis

Statistical analysis was performed using JMP Pro 15 with appropriate parameters as indicated in the figure legends and text. Non-parametric Wilcoxon test was used for gene expression assays, and ANOVA followed by Tukey–Kramer HSD test was used for other assays unless stated otherwise. Different letters or asterisks indicate significant differences according to p-values as indicated in the figure legends.

Accession numbers

Sequence data can be found in the *Arabidopsis* Genome Initiative database under the following accession numbers: *TOC1* (*At5g61380*), *PRR5* (*At5g24470*), *CCA1* (*At2g46830*), *PIF3* (*At1G09530*), *PIF4* (*At2G43010*), *PIF5* (*At3G59060*), *PIL1* (*At2G46970*), *CDF5* (*At1G69570*), *HDA15* (*At3G18520*), *NF-YB2* (*At5G47640*), *NF-YB3* (*At4G14540*), *NF-YC3* (*At1G54830*), *NF-YC4* (*At5G63470*), and *NF-YC9* (*At1G08970*).

Data availability

The mass spectrometry data from this publication have been deposited to the Proteome Exchange database (http://www.proteomexchange.org/) and assigned the identifier PXD026261 (http://proteomecentral.proteomexchange.org/cgi/GetDataset?ID=PXD026261).

Expanded View for this article is available online.

Acknowledgements
This work was supported by the National Institutes of Health (R01GM093285 and R35GM136400 to D.E.S.), the Next-Generation BioGreen21 Program (PJ01327305), the Rural Development Administration, Republic of Korea (to D.E.S.), and the World Class University Program of South Korea (No. R31-2008-000-10105-0), NRF, MEST (to D.E.S.). We thank Dr. Ben Holt III for reagents and early discussions, Dr. Elena Monte for *pif*3/4/5 mutant seeds, and Bohan Liu for assistance with statistical analysis.

Author contributions
JY, SL, YJK, QZ, AR, and LW designed and performed experiments. YN and HN performed the MS analysis. DES conceptualized and supervised the project and wrote the manuscript with JY and comments from the authors.

Conflict of interest
The authors declare that they have no conflict of interest.

References

Bae G, Choi G (2008) Decoding of light signals by plant phytochromes and their interacting proteins. *Annu Rev Plant Biol* 59: 281 – 311

Blau J (2008) PERspective on PER phosphorylation. *Genes Dev* 22: 1737 – 1740

Brenna A, Albrecht U (2020) Phosphorylation and circadian molecular timing. *Front Physiol* 11: 612510

Cao S, Siriwardana CL, Kumimoto RW, Holt III BF (2011) Construction of high quality Gateway entry libraries and their application to yeast two-hybrid for the monocot model plant Brachypodium distachyon. *BMC Biotechnol* 11: 53

Castillon A, Shen H, Huq E (2007) Phytochrome Interacting Factors: central players in phytochrome-mediated light signaling networks. *Trends Plant Sci* 12: 514 – 521

Chaves-Sanjuan A, Gnesutta N, Gobbini A, Martignago D, Bernardini A, Fornara F, Mantovani R, Nardini M (2021) Structural determinants for NF-Y subunit organization and NF-Y/DNA association in plants. *Plant J* 105: 49 – 61

Daniel X, Sugano S, Tobin EM (2004) CK2 phosphorylation of CCA1 is necessary for its circadian oscillator function in *Arabidopsis*. *Proc Natl Acad Sci USA* 101: 3292 – 3297

de Montaigu A, Toth R, Coupland G (2010) Plant development goes like clockwork. *Trends Genet* 26: 296 – 306

Diernfellner AC, Querfurth C, Salazar C, Hofer T, Brunner M (2009) Phosphorylation modulates rapid nucleocytoplasmic shuttling and cytoplasmic accumulation of Neurospora clock protein FRQ on a circadian time scale. *Genes Dev* 23: 2192 – 2200

Dunlap JC (1999) Molecular bases for circadian clocks. *Cell* 96: 271 – 290

Eriksson ME, Hanano S, Southern MM, Hall A, Millar AJ (2003) Response regulator homologues have complementary, light-dependent functions in the *Arabidopsis* circadian clock. *Planta* 218: 159 – 162

Fankhauser C, Casal JJ (2004) Phenotypic characterization of a photomorphogenic mutant. *Plant J* 39: 747 – 760

Fujiwara S, Wang L, Han L, Suh SS, Salome PA, McClung CR, Somers DE (2008) Post-translational regulation of the *Arabidopsis* circadian clock through selective proteolysis and phosphorylation of pseudo-response regulator proteins. *J Biol Chem* 283: 23073 – 23083

Gallego M, Virshup DM (2007) Post-translational modifications regulate the ticking of the circadian clock. *Nat Rev Mol Cell Biol* 8: 139 – 148

Gnesutta N, Kumimoto RW, Swain S, Chiara M, Siriwardana C, Horner DS, Holt III BF, Mantovani R (2017) CONSTANS imparts DNA sequence specificity to the histone fold NF-YB/NF-YC dimer. *Plant Cell* 29: 1516 – 1532

Harmer SL, Panda S, Kay SA (2001) Molecular bases of circadian rhythms. *Annu Rev Cell Dev Biol* 17: 215 – 253

Hou X, Zhou J, Liu C, Liu L, Shen L, Yu H (2014) Nuclear factor Y-mediated H3K27me3 demethylation of the SOC1 locus orchestrates flowering responses of *Arabidopsis*. *Nat Commun* 5: 4601

Huang W, Pérez-García P, Pokhilko A, Millar AJ, Antoshechkin I, Riechmann JL, Mas P (2012) Mapping the core of the Arabidopsis circadian clock defines the network structure of the oscillator. *Science* 336: 75 – 79

Ishihama Y, Rappsilber J, Andersen JS, Mann M (2002) Microcolumns with self-assembled particle frits for proteomics. *J Chromatogr A* 979: 233 – 239

Ito S, Nakamichi N, Kiba T, Yamashino T, Mizuno T (2007) Rhythmic and light-inducible appearance of clock-associated pseudo-response regulator protein PRR9 through programmed degradation in the dark in *Arabidopsis thaliana*. *Plant Cell Physiol* 48: 1644 – 1651

Ito S, Niwa Y, Nakamichi N, Kawamura H, Yamashino T, Mizuno T (2008) Insight into missing genetic links between two evening-expressed pseudo-response regulator genes TOC1 and PRR5 in the circadian clock-controlled circuitry in *Arabidopsis thaliana*. *Plant Cell Physiol* 49: 201 – 213

Jiao Y, Lau OS, Deng XW (2007) Light-regulated transcriptional networks in higher plants. *Nat Rev Genet* 8: 217 – 230

Kikis EA, Khanna R, Quail PH (2005) ELF4 is a phytochrome-regulated component of a negative-feedback loop involving the central oscillator components CCA1 and LHY. *Plant J* 44: 300 – 313

Kim WY, Fujiwara S, Suh SS, Kim J, Kim Y, Han L, David K, Putterill J, Nam HG, Somers DE (2007) ZEITLUPE is a circadian photoreceptor stabilized by GIGANTEA in blue light. *Nature* 449: 356 – 360

Kumimoto RW, Zhang Y, Siefers N, Holt III BF (2010) NF-YC3, NF-YC4 and NF-YC9 are required for CONSTANS-mediated, photoperiod-dependent flowering in *Arabidopsis thaliana*. *Plant J* 63: 379 – 391

Leivar P, Quail PH (2011) PIFs: pivotal components in a cellular signaling hub. *Trends Plant Sci* 16: 19 – 28

Li N, Zhang Y, He Y, Wang Y, Wang L (2020) Pseudo response regulators regulate photoperiodic hypocotyl growth by repressing PIF4/5 transcription. *Plant Physiol* 183: 686 – 699

Liu TL, Newton L, Liu MJ, Shiu SH, Farre EM (2016) A G-Box-like motif is necessary for transcriptional regulation by circadian pseudo-response regulators in *Arabidopsis*. *Plant Physiol* 170: 528 – 539

Liu X, Chen CY, Wang KC, Luo M, Tai R, Yuan L, Zhao M, Yang S, Tian G, Cui Y *et al* (2013) PHYTOCHROME INTERACTING FACTOR 3 associates with the histone deacetylase HDA15 in repression of chlorophyll biosynthesis and photosynthesis in etiolated *Arabidopsis* seedlings. *Plant Cell* 25: 1258 – 1273

Lv X, Zeng X, Hu H, Chen L, Zhang F, Liu R, Liu Y, Zhou X, Wang C, Wu Z *et al* (2021) Structural insights into the multivalent binding of the *Arabidopsis* FLOWERING LOCUS T promoter by the CO–NF–Y master transcription factor complex. *Plant Cell* 33: 1182 – 1195

Martín G, Rovira A, Veciana N, Soy J, Toledo-Ortiz G, Gommers CMM, Boix M, Henriques R, Minguet EG, Alabadí D *et al* (2018) Circadian waves of transcriptional repression shape PIF-regulated photoperiod-responsive growth in *Arabidopsis*. *Curr Biol* 28: 311 – 318

Mohannath G, Jackel JN, Lee YH, Buchmann RC, Wang H, Patil V, Adams AK, Bisaro DM (2014) A complex containing SNF1-related kinase (SnRK1) and adenosine kinase in *Arabidopsis*. *PLoS One* 9: e87592

Myers ZA, Holt III BF (2018) NUCLEAR FACTOR-Y: still complex after all these years? *Curr Opin Plant Biol* 45: 96 – 102

Myers ZA, Kumimoto RW, Siriwardana CL, Gayler KK, Risinger JR, Pezzetta D, Holt Iii BF (2016) NUCLEAR FACTOR Y, Subunit C (NF-YC) transcription factors are positive regulators of photomorphogenesis in *Arabidopsis thaliana*. *PLoS Genet* 12: e1006333

Niwa Y, Yamashino T, Mizuno T (2009) The circadian clock regulates the photoperiodic response of hypocotyl elongation through a coincidence mechanism in *Arabidopsis thaliana*. *Plant Cell Physiol* 50: 838 – 854

Nohales MA, Liu W, Duffy T, Nozue K, Sawa M, Pruneda-Paz JL, Maloof JN, Jacobsen SE, Kay SA (2019) Multi-level modulation of light signaling by GIGANTEA regulates both the output and pace of the circadian clock. *Dev Cell* 49: 840 – 851

Nomoto Y, Kubozono S, Yamashino T, Nakamichi N, Mizuno T (2012) Circadian clock- and PIF4-controlled plant growth: a coincidence mechanism directly integrates a hormone signaling network into the photoperiodic control of plant architectures in *Arabidopsis thaliana*. *Plant Cell Physiol* 53: 1950 – 1964

Nomoto Y, Kubozono S, Miyachi M, Yamashino T, Nakamichi N, Mizuno T (2013) Circadian clock and PIF4-mediated external coincidence mechanism coordinately integrates both of the cues from seasonal changes in photoperiod and temperature to regulate plant growth in *Arabidopsis thaliana*. *Plant Signal Behav* 8: e22863

Nozue K, Covington MF, Duek PD, Lorrain S, Fankhauser C, Harmer SL, Maloof JN (2007) Rhythmic growth explained by coincidence between internal and external cues. *Nature* 448: 358 – 361

Nusinow DA, Helfer A, Hamilton EE, King JJ, Imaizumi T, Schultz TF, Farre EM, Kay SA (2011) The ELF4-ELF3-LUX complex links the circadian clock to diurnal control of hypocotyl growth. *Nature* 475: 398 – 402

Okuda S, Watanabe YU, Moriya Y, Kawano S, Yamamoto T, Matsumoto M, Takami T, Kobayashi D, Araki N, Yoshizawa AC *et al* (2017) jPOSTrepo: an international standard data repository for proteomes. *Nucleic Acids Res* 45: D1107 – D1111

Olsen JV, de Godoy LM, Li G, Macek B, Mortensen P, Pesch R, Makarov A, Lange O, Horning S, Mann M (2005) Parts per million mass accuracy on an Orbitrap mass spectrometer via lock mass injection into a C-trap. *Mol Cell Proteomics* 4: 2010 – 2021

Olsen JV, Ong SE, Mann M (2004) Trypsin cleaves exclusively C-terminal to arginine and lysine residues. *Mol Cell Proteomics* 3: 608 – 614

Para A, Farre EM, Imaizumi T, Pruneda-Paz JL, Harmon FG, Kay SA (2007) PRR3 Is a vascular regulator of TOC1 stability in the *Arabidopsis* circadian clock. *Plant Cell* 19: 3462 – 3473

Petroni K, Kumimoto RW, Gnesutta N, Calvenzani V, Fornari M, Tonelli C, Holt III BF, Mantovani R (2012) The promiscuous life of plant NUCLEAR FACTOR Y transcription factors. *Plant Cell* 24: 4777 – 4792

Pham VN, Kathare PK, Huq E (2018) Phytochromes and phytochrome interacting factors. *Plant Physiol* 176: 1025 – 1038

Rappsilber J, Ishihama Y, Mann M (2003) Stop and go extraction tips for matrix-assisted laser desorption/ionization, nanoelectrospray, and LC/MS sample pretreatment in proteomics. *Anal Chem* 75: 663 – 670

Ravichandran A, Sugiyama N, Tomita M, Swarup S, Ishihama Y (2009) Ser/Thr/Tyr phosphoproteome analysis of pathogenic and non-pathogenic Pseudomonas species. *Proteomics* 9: 2764 – 2775

Roenneberg T, Foster RG (1997) Twilight times: light and the circadian system. *Photochem Photobiol* 66: 549 – 561

Saini R, Jaskolski M, Davis SJ (2019) Circadian oscillator proteins across the kingdoms of life: structural aspects. *BMC Biol* 17: 13

Schroeder MJ, Shabanowitz J, Schwartz JC, Hunt DF, Coon JJ (2004) A neutral loss activation method for improved phosphopeptide sequence analysis by quadrupole ion trap mass spectrometry. *Anal Chem* 76: 3590 – 3598

Schweiger R, Linial M (2010) Cooperativity within proximal phosphorylation sites is revealed from large-scale proteomics data. *Biol Direct* 5: 6

Seo PJ, Mas P (2014) Multiple layers of posttranslational regulation refine circadian clock activity in *Arabidopsis*. *Plant Cell* 26: 79 – 87

Shen C, Liu H, Guan Z, Yan J, Zheng T, Yan W, Wu C, Zhang Q, Yin P, Xing Y (2020) Structural insight into DNA recognition by CCT/NF-YB/YC complexes in plant photoperiodic flowering. *Plant Cell* 32: 3469 – 3484

Shevchenko A, Tomas H, Havlis J, Olsen JV, Mann M (2006) In-gel digestion for mass spectrometric characterization of proteins and proteomes. *Nat Protoc* 1: 2856 – 2860

Somers DE, Kim WY, Geng R (2004) The F-box protein ZEITLUPE confers dosage-dependent control on the circadian clock, photomorphogenesis, and flowering time. *Plant Cell* 16: 769 – 782

Soy J, Leivar P, Gonzalez-Schain N, Martin G, Diaz C, Sentandreu M, Al-Sady B, Quail PH, Monte E (2016) Molecular convergence of clock and photosensory pathways through PIF3-TOC1 interaction and co-occupancy of target promoters. *Proc Natl Acad Sci USA* 113: 4870 – 4875

Sugano S, Andronis C, Green RM, Wang ZY, Tobin EM (1998) Protein kinase CK2 interacts with and phosphorylates the *Arabidopsis* circadian clock-associated 1 protein. *Proc Natl Acad Sci USA* 95: 11020 – 11025

Tang Y, Liu X, Liu X, Li Y, Wu K, Hou X (2017) *Arabidopsis* NF-YCs mediate the light-controlled hypocotyl elongation via modulating histone acetylation. *Mol Plant* 10: 260 – 273

Uehara TN, Mizutani Y, Kuwata K, Hirota T, Sato A, Mizoi J, Takao S, Matsuo H, Suzuki T, Ito S *et al* (2019) Casein kinase 1 family regulates PRR5 and TOC1 in the *Arabidopsis* circadian clock. *Proc Natl Acad Sci USA* 116: 11528 – 11536

Wang L, Fujiwara S, Somers DE (2010) PRR5 regulates phosphorylation, nuclear import and subnuclear localization of TOC1 in the *Arabidopsis* circadian clock. *EMBO J* 29: 1903 – 1915

Wang L, Kim J, Somers DE (2013) Transcriptional corepressor TOPLESS complexes with pseudoresponse regulator proteins and histone deacetylases to regulate circadian transcription. *Proc Natl Acad Sci USA* 110: 761 – 766

Wenkel S, Turck F, Singer K, Gissot L, Le Gourrierec J, Samach A, Coupland G (2006) CONSTANS and the CCAAT box binding complex share a functionally important domain and interact to regulate flowering of *Arabidopsis*. *Plant Cell* 18: 2971 – 2984

Yakir E, Hilman D, Harir Y, Green RM (2007) Regulation of output from the plant circadian clock. *FEBS J* 274: 335 – 345

Yamaguchi N, Winter CM, Wu MF, Kwon CS, William DA, Wagner D (2014) PROTOCOLS: chromatin immunoprecipitation from *Arabidopsis* tissues. *Arabidopsis Book* 12: e0170

Yan J, Kim YJ, Somers DE (2021) Post-translational mechanisms of plant circadian regulation. *Genes (Basel)* 12: 325

Yoo SD, Cho YH, Sheen J (2007) *Arabidopsis* mesophyll protoplasts: a versatile cell system for transient gene expression analysis. *Nat Protoc* 2: 1565 – 1572

Zhai Z, Jung HI, Vatamaniuk OK (2009) Isolation of protoplasts from tissues of 14-day-old seedlings of *Arabidopsis thaliana*. *J uis Exp*

Zhang Y, Pfeiffer A, Tepperman JM, Dalton-Roesler J, Leivar P, Gonzalez Grandio E, Quail PH (2020) Central clock components modulate plant shade avoidance by directly repressing transcriptional activation activity of PIF proteins. *Proc Natl Acad Sci USA* 117: 3261 – 3269

Zhao H, Wu D, Kong F, Lin K, Zhang H, Li G (2016) The *Arabidopsis thaliana* nuclear factor Y transcription factors. *Front Plant Sci* 7: 2045

Zhu JY, Oh E, Wang T, Wang ZY (2016) TOC1-PIF4 interaction mediates the circadian gating of thermoresponsive growth in *Arabidopsis*. *Nat Commun* 7: 13692